

UNCLASSIFIED

AD NUMBER

AD830463

LIMITATION CHANGES

TO:

Approved for public release; distribution is unlimited.

FROM:

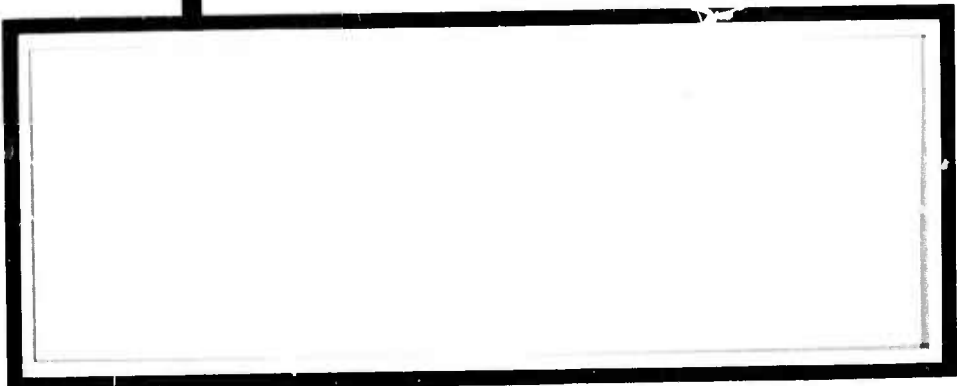
Distribution authorized to U.S. Gov't. agencies and their contractors; Critical Technology; FEB 1968. Other requests shall be referred to Air Force Technical Application Center, Washington, DC 20333. This document contains export-controlled technical data.

AUTHORITY

usaf ltr, 25 jan 1972

THIS PAGE IS UNCLASSIFIED

AD830463



D D C
RECEIVED
APR 22 1968
RECEIVED
C

STATEMENT #2 UNCLASSIFIED

This document is subject to special export controls and each
transmittal to foreign governments or foreign nationals may be
made only with prior approval of AF Technical Applications Center

Attn: VSC, Washington, D.C. 20333



TEXAS INSTRUMENTS

SCIENCE SERVICES DIVISION

1100 NORTH CENTRAL EXPRESSWAY
DALLAS, TEXAS



VELA T/7701

NETWORK STUDIES - SIGNAL CHARACTERISTICS

ADVANCED ARRAY RESEARCH

Special Report No. 7

Prepared by

Stephen A. Benno Peter L. Strange
William A. Johnson James A. Bonner

John P. Burg, Program Scientist
George D. Hair, Program Manager
Telephone: 1-214-238-3473

TEXAS INSTRUMENTS INCORPORATED

Science Services Division

P. O. Box 5621
Dallas, Texas 75222

Contract: F33657-67-C-0708-P001
Contract Date: 15 December 1966
Amount of Contract: \$ 625, 500
Contract Expiration Date: 14 December 1967

Sponsored by

ADVANCED RESEARCH PROJECTS AGENCY

Nuclear Test Detection Office

ARPA Order No. 624

ARPA Program Code No. 7F10

15 February 1968



ACKNOWLEDGMENT

This research was supported by the
ADVANCED RESEARCH PROJECTS AGENCY
Nuclear Test Detection Office
under Project VELA UNIFORM
and accomplished under the technical direction of the
AIR FORCE TECHNICAL APPLICATIONS CENTER
under Contract No. F33657-67-C-0708-P001



ABSTRACT

This report presents an initial study of signal characteristics and coherent signal processing at the network level. Topics investigated include signal similarity, depth-phase detection and recognition, separation and location of events overlapping in time and space, and methods for real-time network processing and data presentation.

Large variations in signal waveform and signal-to-noise ratio (SNR) are observed across the network. Interstation coefficients of correlation for a relatively simple Kamchatka event vary from 0.54 to 0.96, with the higher correlation found for stations on the eastern North American continent. Levinson equalization filtering does not appear particularly effective at the network level in terms of improved correlation coefficients or SNR. Depth-phase detection at the network level is not materially better than for selected stations, but recognition appears more reliable than for station results in general. Experiments show that overlapping events of differing magnitudes and separated in epicenter by as little as 1° can be resolved by network beamsteer and integrate techniques. Signal-enhancement procedures implemented primarily to determine the extent of signal attenuation caused by signal dissimilarity across the network indicate less than 3-db reduction in signal energy across the signal passband (for an 8-station network). Ambient noise levels and scattered signal in the P coda are reduced by 7 to 9 db, as expected for uncorrelated energy. A method of weighting stations by their SNR's emphasizes the stations with better signal estimates and yields an additional 4- to 7-db improvement in SNR at the network level.



LIST OF ACRONYMS AND SPECIAL SYMBOLS

ADIS	Network station, Adak, Aleutian Islands
BS	Beamsteer
C	Coda power spectrum
CPO	Cumberland Plateau Observatory, McMinnville, Tennessee
DHNY	Network station, Delhi, New York
GGGR	Network station, Grafenburg, West Germany
HWIS	Network station, Hawaiian Islands
LE	Beamsteer of Levinson-equalized data
LZBV	Network station, LaPaz, Bolivia
N	Noise spectrum
NPNT	Network station, Mould Bay, N. W. Territory
OONW	Network station, Oslo, Norway
P	Power spectrum
ARKON	Network station, Red Lake, Ontario
RMS	Root-mean-square
SNR	Signal-to-noise ratio
SNW	Signal-to-noise -ratio weighted beamsteer
TFO	Tonto Forest Observatory, Payson, Arizona
USC&GS	United States Coast and Geodetic Survey



TABLE OF CONTENTS

Section	Title	Page
	ABSTRACT	iii
I	INTRODUCTION AND SUMMARY	I-1
II	DESCRIPTION OF DATA AND ARRAYS	II-1
III	STUDIES OF NETWORK SIGNAL SIMILARITY	III-1
IV	PHASE EXTRACTION STUDY	IV-1
V	SIGNAL SEPARATION STUDY	V-1
VI	EVALUATION OF A TECHNIQUE FOR WORLDWIDE COHERENT ENERGY ANALYSIS	VI-1

LIST OF TABLES

Table	Title	Page
II-1	Event Description	II-6
II-2	Network Stations	II-6
III-1	Peak Signal-To-RMS-Noise-Ratio Improvements for Network-Processing Techniques	III-8



LIST OF ILLUSTRATIONS

Figure	Description	Page
II-1	Subarray Straight Sums for Kamchatka Event	II-2
II-2	Subarray Straight Sums for Kurile-1 Event	II-3
II-3	Subarray Straight Sums for Kurile-2 Event	II-4
II-4	Subarray Straight Sums for Kurile-3 Event	II-5
III-1	Kamchatka Interstation Correlation Coefficients	III-2
III-2	Levinson-Filtered Equalization of Kamchatka Event to TFO Trace	III-4
III-3	Levinson-Filtered Equalization of Kurile-2 Event to NPNT Trace	III-5
III-4	Kamchatka Event Network Beamsteer Outputs for Four Preprocessing Schemes	III-6
III-5	Kurile-2 Event Network Beamsteer Outputs for Four Preprocessing Schemes	III-7
III-6	Kamchatka and Kurile-2 Spectral Ratios Between Average Input Trace and Beamsteer Output Relative to Unity	III-11
III-7	Kamchatka and Kurile-2 Spectral Ratios for Network Outputs Compared to an Average Input Trace	III-12
III-8	Kamchatka Signal-to-Noise-Ratio Improvements for Network Processing	III-15
III-9	Kurile-2 Signal-to-Noise-Ratio Improvements for Network Processing	III-17
IV-1	Kamchatka P-30 Correlations and Average Aligned on USC&GS pP	IV-4
IV-2	Kamchatka Smoothed P-30 Correlations and Average Aligned on USC&GS pP	IV-5
IV-3	Kurile-1 P-30 Correlations and Average Aligned on USC&GS pP	IV-7
IV-4	Kurile-1 Smoothed P-30 Correlations and Average Aligned on USC&GS pP	IV-7
IV-5	Kurile-1 Smoothed Time Traces and Average Aligned on USC&GS pP	IV-8



LIST OF ILLUSTRATIONS (CONTD)

Figure	Description	Page
IV-6	Kurile-2 P-30 Correlations and Average Aligned on USC&GS pP	IV-9
IV-7	Kurile-2 Smoothed P-30 Correlations and Average Aligned on USC&GS pP	IV-10
IV-8	Kurile-2 Smoothed Time Traces and Average Aligned on USC&GS pP	IV-12
IV-9	Kurile-3 P-30 Correlations and Average Aligned on USC&GS pP	IV-13
IV-10	Kurile-3 Smoothed P-30 Correlations and Average Aligned on USC&GS pP	IV-13
IV-11	Kurile-3 Smoothed Time Traces and Average Aligned on USC&GS pP	IV-14
V-1	Case A — 8-Station Recordings of 5.8-Magnitude Earthquakes	V-4
V-2	Case B — Simulated 8-Station Recording of Two 5.8-Magnitude Earthquakes Occurring Simultaneously and 1° Apart	V-5
V-3	Case C — Simulated 8-Station Recording of 5.8- and 5.3-Magnitude Earthquakes Occurring Simultaneously and 1° Apart	V-6
V-4	Case D — Simulated 8-Station Recording of Two 5.8-Magnitude Earthquakes Occurring 10-sec Apart and 1° Apart	V-7
V-5	Case E — Simulated 8-Station Recording of 5.8- and 5.3-Magnitude Earthquakes Occurring 10-sec Apart and 1° Apart	V-8
V-6	8-Station Smoothed Beamsteer Network Outputs for Case A	V-9
V-7	8-Station Smoothed Beamsteer Network Outputs for Case B	V-9
V-8	8-Station Smoothed Beamsteer Network Outputs for Case C	V-10
V-9	8-Station Smoothed Beamsteer Network Outputs for Case D	V-10
V-10	8-Station Smoothed Beamsteer Network Outputs for Case E	V-11
V-11	Beamsteered Plots for Five Time Traces for Case A	V-13



LIST OF ILLUSTRATIONS (CONTD)

Figure	Description	Page
V-12	Beamsteered Plots for Five Time Traces for Case B	V-15
V-13	Beamsteered Plots for Five Time Traces for Case C	V-17
V-14	Beamsteered Plots for Five Time Traces for Case D	V-19
V-15	Beamsteered Plots for Five Time Traces for Case E	V-21
VI-1	Worldwide Spectrum, Short-Period Equalized Signal	VI-6
VI-2	Worldwide Spectrum, Long-Period Equalized Signal	VI-6
VI-3	Worldwide Spectrum, Long-Period Equalized Signal with Time Residuals	VI-7
VI-4	Worldwide Spectrum, Long-Period Equalized Signal with Existing 10-Station Network	VI-7
VI-5	Worldwide Spectrum, Two Time-Overlapping Short-Period Equalized Signals	VI-8



SECTION I INTRODUCTION AND SUMMARY

Significant advances in seismic signal enhancement and identification have been achieved through the recording and coherent processing of seismic array data. An even more powerful approach is the extension of coherent processing and analysis to data recorded by a network of array stations. Consequently, as part of this project, a study was initiated 1 year ago to characterize the worldwide ambient noise field and seismic signals seen by a network. Results of this initial study of signal characteristics and their significance to coherent network processing for seismic event detection and identification are contained in this report. Special Report No. 6 contains results of the initial study of worldwide ambient-noise-field characteristics.*

Signal characteristics of interest include

- P-wave waveform, amplitude, and frequency content similarity
- Consistency of identifiable depth phases
- Differences between earthquake and explosion signals uniquely measurable with a network
- Consistency of recording station effects such as earth filtering, time anomalies, and multipaths

*Texas Instruments Incorporated, 1968: Network Studies — Noise Characteristics, Advanced Array Research Spec. Rpt. No. 6, Contract F33657-67-C-0708, 15 Feb.



The capability of a network to perform certain functions is very much dependent on these signal characteristics, so several experiments to estimate the effectiveness of network processing were performed. Those functions investigated were the network's ability to

- Improve evidence of and positively identify depth phases
- Resolve events closely spaced in time and epicenter
- Extract P-waves for improved estimates of relative frequency content and P-coda complexity for more positive source identification
- Perform continuous real-time monitoring of worldwide seismic activity

This initial study was necessarily rather limited in scope, and some network signal characteristics such as differences between earthquake and explosion signals were not studied. Although simultaneous recordings of several signals were obtained, only two signals were examined in detail. No suitable network recordings of explosion events were obtained in time to permit their analysis. Thus, the findings and conclusions of this study must be considered preliminary and subject to later modification when more events have been examined.

The study can be discussed best in terms of the experiments designed to determine the effects of network signal characteristics on the four network functions previously mentioned. The following paragraphs summarize the objectives and results of these experiments.

In the depth-phase-extraction experiment, four events were processed to investigate the capability of network processing for depth-phase enhancement. In general, results of the experiment showed good indications



of depth phases following network processing. While depth phases were not more evident on the network outputs than at some stations, depth phases definitely were detected with network processing although not detectable at many individual stations.

The overlapping-signal-resolution study was performed to determine the ability of a limited network to separate time-overlapping events. The experiment showed that a limited 8-station network can successfully separate two time-overlapping events with relative magnitude differences of one-half a magnitude unit, even when separated by as little as 1° in epicenter. The lower-magnitude event in this study was a relatively simple event and the higher-magnitude event relatively complex. It is felt that events with larger-magnitude differences could be resolved if epicenter separations were larger or if the number of stations and size of the network were increased. Therefore, network processing offers a solution to the problem of event concealment, as well as improved resolution in epicentral determination.

Two events were processed at the network level to determine the extent of the signal-similarity problem. The signals were examined through computation of interstation correlation coefficients, visual analysis, design of specific Levinson equalization filters, and the relative performance of several elementary processing procedures such as simple and weighted beamsteers. The effects of certain types of network processing on P-wave, P-coda, noise and event complexity were analyzed through measurements of peak signal-to-RMS-noise ratios (SNR) and broadband signal-to-noise power ratio improvement as a function of frequency.

Appreciable dissimilarities in signal waveform and station SNR's were observed across the network for the two events. Correlation coefficients for the relatively simple Kamchatka event range from 0.52 to 0.96, with stations on the eastern North American continent showing highest interstation correlation. Improvements in SNR using Levinson-equalized data were generally no greater than those achieved with simple beamsteering, and such equalization does not appear particularly promising for network data.



Spectra from a simple beamsteer (visual signal alignment) of network data were compared with average station spectra, and results indicated

- Signal loss which averaged approximately 3 db at the peak-signal frequency
- Broadband noise power reduction of 9 db (using 8 stations)
- SNR improvements of 7 to 13 db within the signal band
- Broadband attenuation of scattered signal energy and noise power within the P-coda averaging 8 db

The beamsteering experiments were performed primarily to study the effect on network signal characteristics rather than for signal determination. Network processing does not appear particularly advantageous for signal detection, but a worldwide distribution of stations should give more effective coverage than a single station.

The fourth experiment evaluated a simple technique for worldwide coherent-energy measurement. Results showed that the technique can locate equalized short- and long-period signals correctly and that time anomalies do not appreciably affect event location when using long-period data. For nonequalized signals and multiple events, the presence of spectral sidelobes prevents correct event location. The experiment demonstrates that network data can be processed in real-time and that this processing can produce simple forms of data presentation which could be used to monitor worldwide seismic activity continuously.



Network processing appears to be advantageous in the following areas:

- Signal extraction

Network processing produces improved resolution in an epicentral location. Network processing can effectively separate time-overlapping events for which the epicenters are less than 1° apart and for which the difference in magnitudes is at least one-half unit.

- Event classification

By reducing the scattered signal energy within the P-coda, network processing can produce more consistent measurements of spectral content and event complexity than can be obtained at the station level. Network processing produces reliable and consistent indications of depth phases for events for which depth phases would not be detectable at many of the network stations.

- Worldwide seismic monitoring

Real-time network processing can detect and correctly locate seismic events, is not affected by time anomalies when using long-period data, requires very little computer time, and is ideally suited for necessary display and monitoring techniques.

Based on these observations, it is felt that additional investigations of network signal characteristics and signal processing are warranted. Both long- and short-period recordings of a much larger number of events should be analyzed. Explosion as well as earthquake events should be included to produce quantitative measurements of network-processing potential for event classification. Such studies could be considerably improved by using larger networks consisting of more seismic stations and possibly by using advanced processing techniques (e. g., Wiener or adaptive MCF) at the individual array-station level.

BLANK PAGE



SECTION II

DESCRIPTION OF DATA AND ARRAYS

Four events from a library of 12 were chosen for processing in this initial phase of network studies. The choice of the events to be used was based on the number of available station recordings, quality of data, event SNR, and presence of possible depth phases.

The results of processing the four events are shown in Figures II-1 through II-4. The traces shown are either single-seismometer outputs or averages (for array stations) and have been normalized for plotting. Table II-1 gives a brief description of the four events.

The location of each station and the number of short-period vertical seismometers at each station are presented in Table II-2. A more detailed description of the stations and their array geometries is presented in a Special Report No. 6.*

*Ibid.

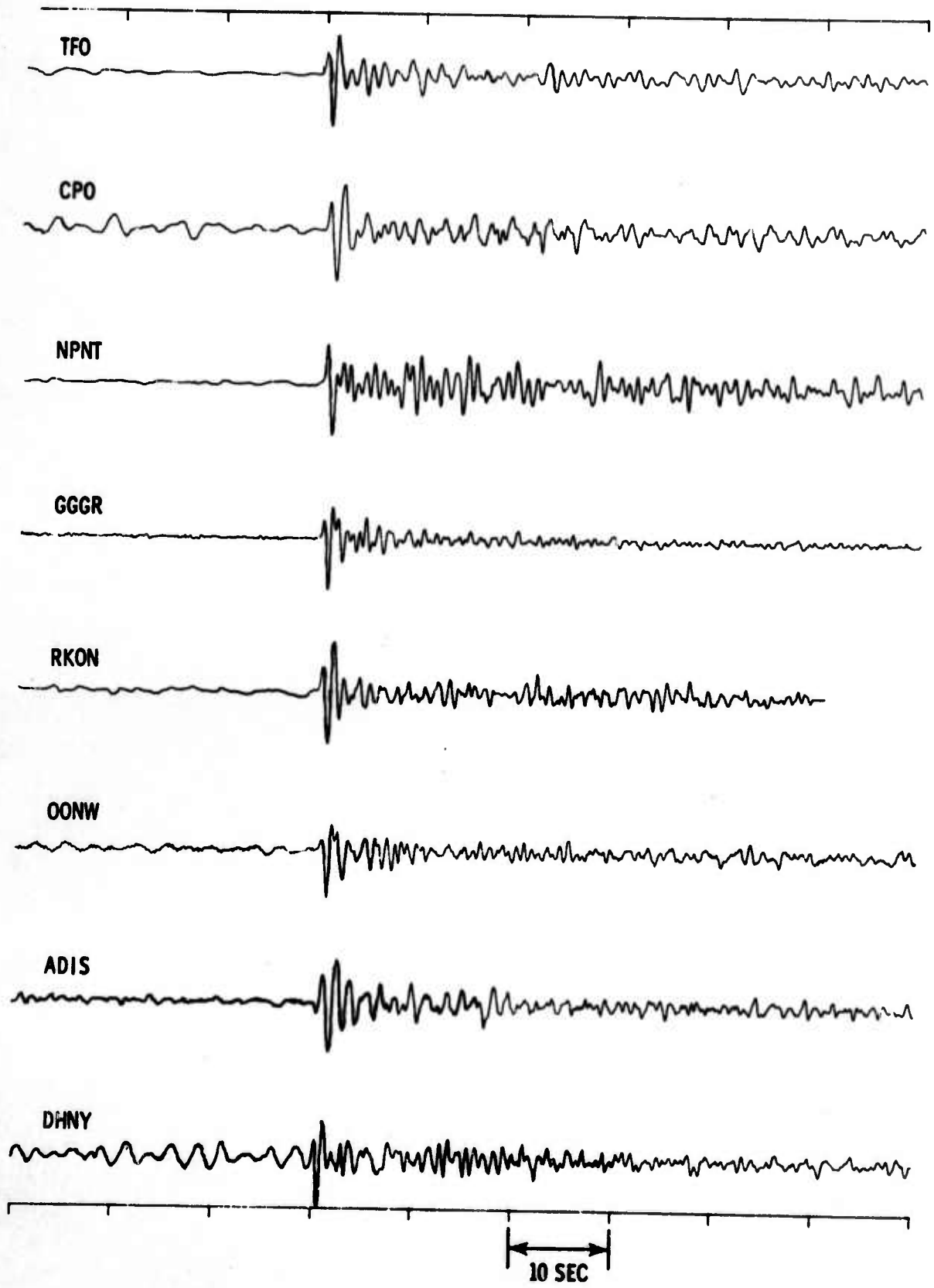


Figure II-1. Subarray Straight Sums for Kamchatka Event

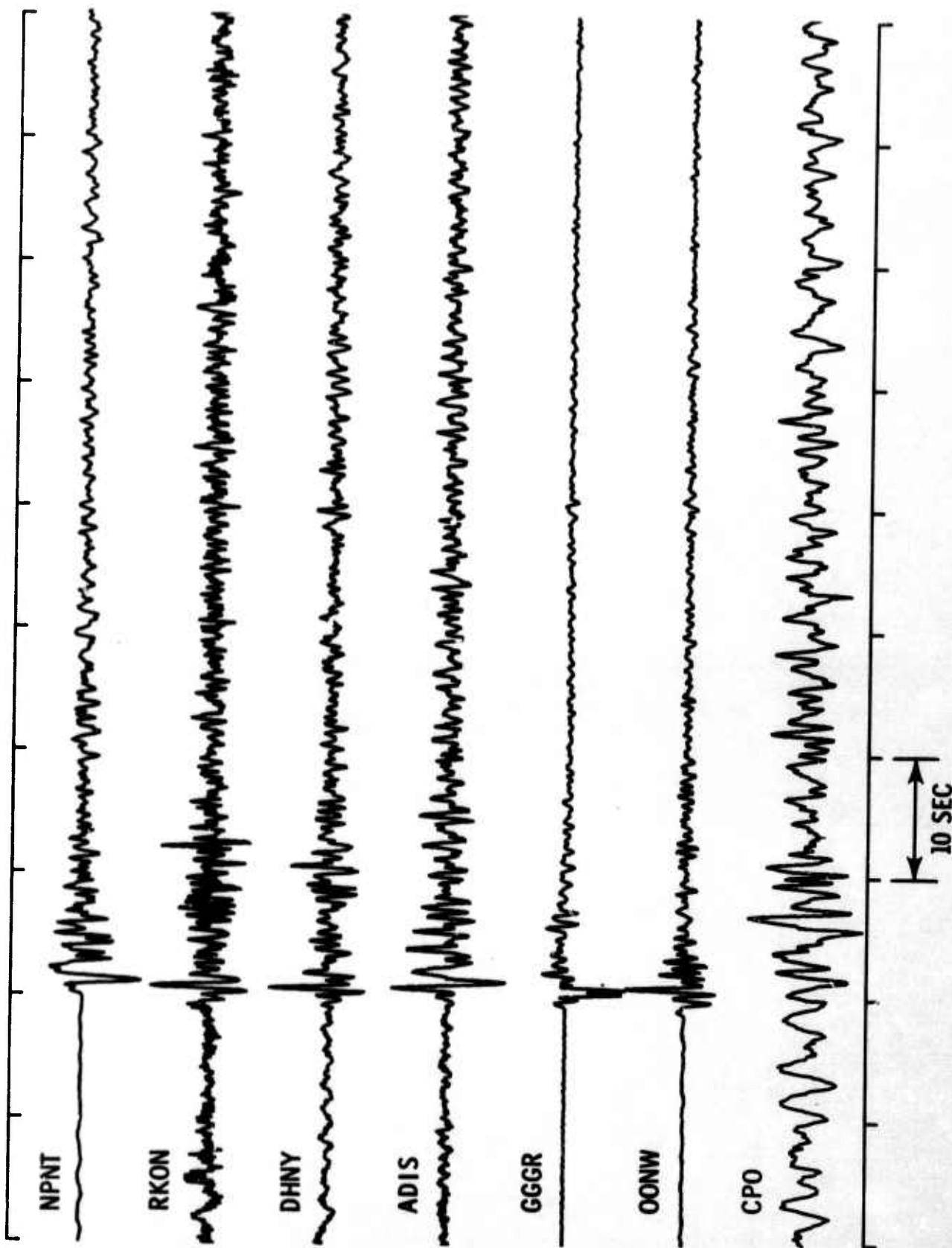


Figure II-2. Subarray Straight Sums for Kurile-1 Event

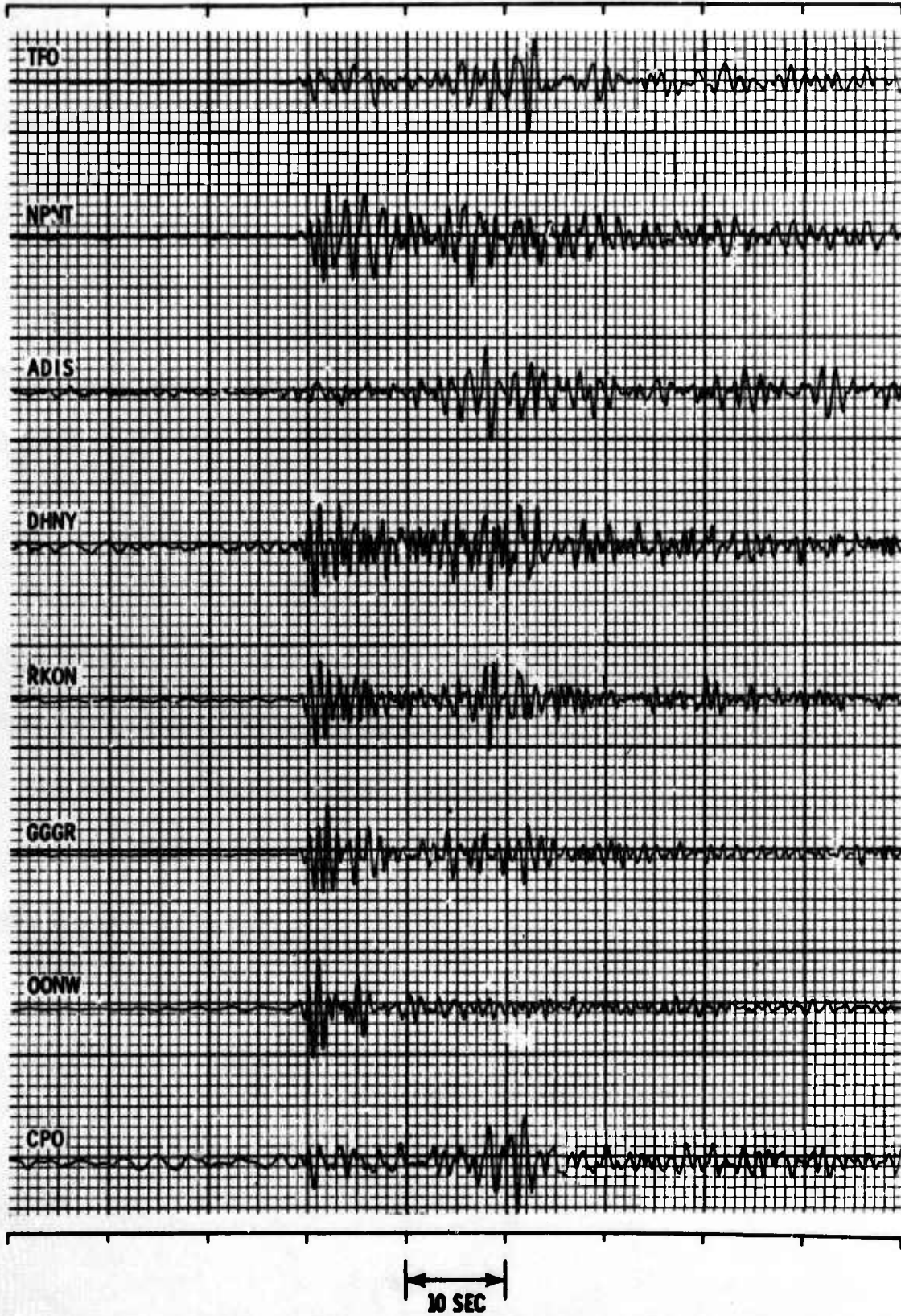


Figure II-3. Subarray Straight Sums for Kurile-2 Event

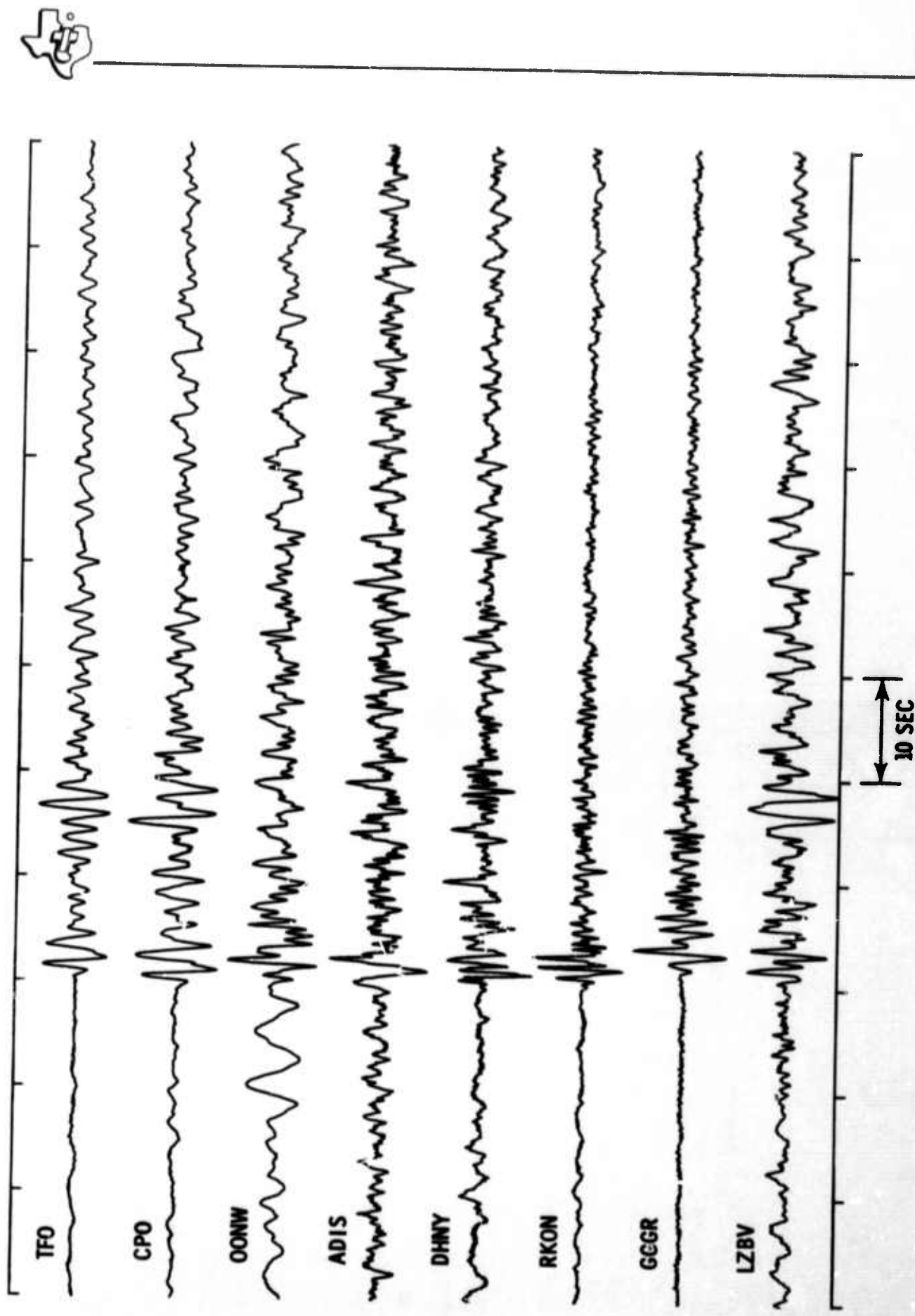


Figure II-4. Subarray Straight Sums for Kurile-3 Event



Table II-1
EVENT DESCRIPTION

Event	Date	Time	Lat. (°N)	Long. (°E)	Depth (km)	Mag. (m_b)	No. of Stations
Kamchatka	29 Jan 1965	9:35:25.7	54.8	161.7	33	5.8	8
Kurile 1	12 Aug 1964	6:51:49.9	48.9	153.7	127	5.6	7
Kurile 2	16 Oct 1964	6:59:38.6	44.3	149.5	33	5.5	8
Kurile 3	6 Nov 1964	9:53:22.4	44.4	149.0	60	5.7	8

Table II-2
NETWORK STATIONS

Station Designation	Station Location	No. of Seismometers Used
ADIS	Adak, Aleutian Islands	1
CPO	McMinnville, Tennessee	10
DHNY	Delhi, New York	1
GGGR	Grafenau, West Germany	7
HWIS	Hawaiian Islands	14
LZBV	LaPaz, Bolivia	7
NPNT	Mould Bay, N.W. Territory	7
OONW	Oslo, Norway	7
RKON	Red Lake, Ontario	1
TFO	Payson, Arizona	11



SECTION III

STUDIES OF NETWORK SIGNAL SIMILARITY

Extent of the signal similarity across the network is of primary importance to network-processing procedures. The complexity of required network processing can be significantly reduced if this similarity is high. Several approaches were taken to investigate signal similarity. These include visual analysis, interstation correlation coefficients, design and application of specific Levinson filters, and the implementation of several elementary network-processing procedures to estimate signal attenuation.

The Kamchatka event (Figure II-1) was chosen for processing because of its relative simplicity and waveform similarity among stations. Kurile Islands event 2 (Figure II-3) was chosen for its complexity in order to provide a contrast with the Kamchatka event.

Large differences between stations for both the P-phase and later-arriving phases were observed. Differing SNR's were also evident even after allowing for improvements from array-station preprocessing (averaging). Across the network, station SNR's varied by as much as 18 db. As a quantitative measure of waveform similarity, the relatively simple Kamchatka event, which appeared most similar between stations, was analyzed through the computation of interstation correlation coefficients (Figure III-1). Values obtained ranged from 0.52 to 0.96, suggesting a considerable lack of similarity even for this simple event. Stations DHNY, RKON, and CPO generally were more highly correlated, probably because all stations are relatively close and all are on the eastern North American continent. DHNY appears to correlate best with all stations and emphasizes the need for proper choice of reference station if signal equalization is required.

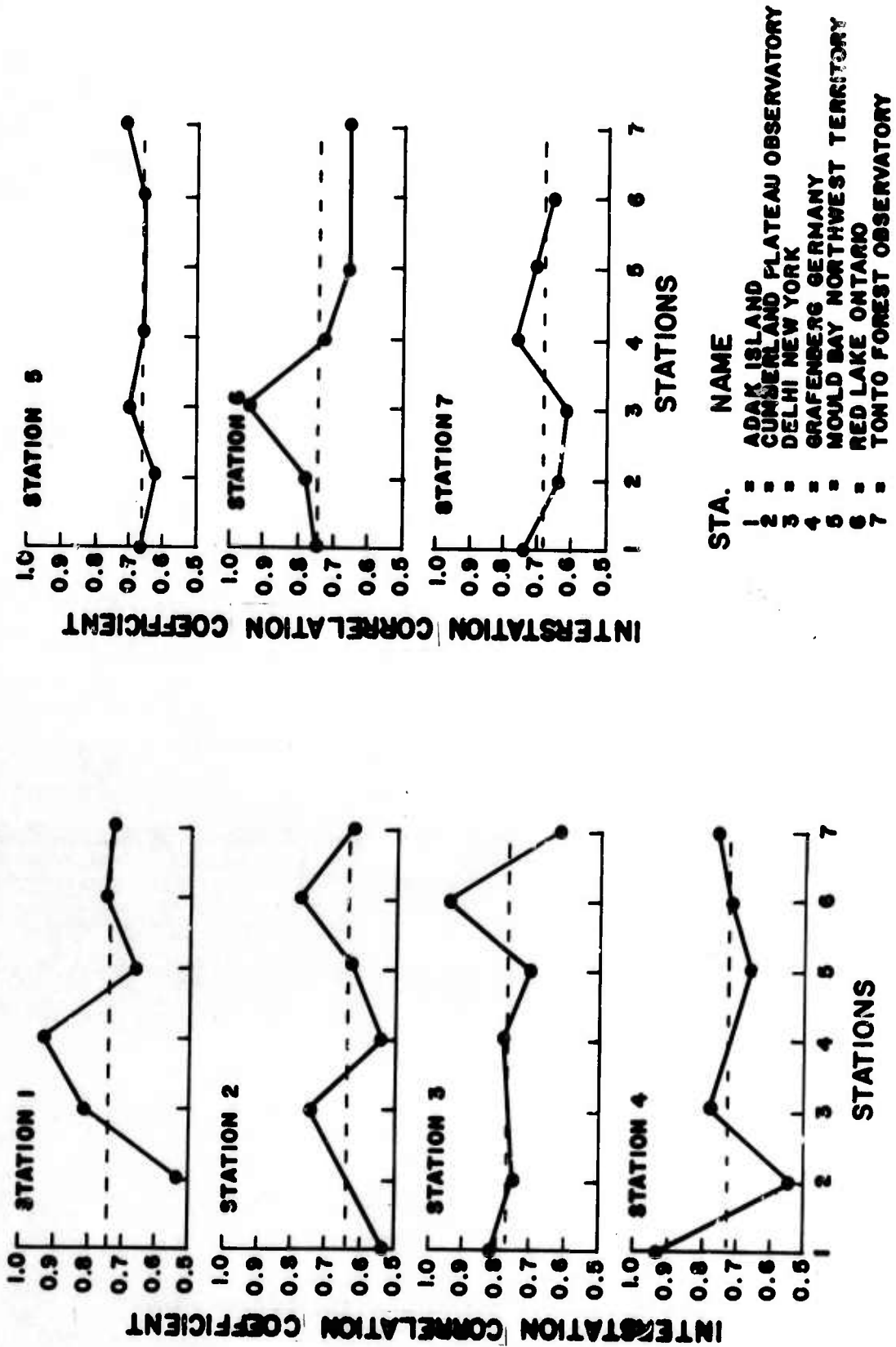


Figure III-1. Kamchatka Interstation Correlation Coefficients



To determine if signal dissimilarity could be reduced, 2.5-sec Levinson equalization filters were designed from 5.0 sec of bandlimited signal (0.8- to 2.8-Hz 0-phase filter) and applied to the design event. For the Kamchatka event, all stations were equalized to TFO. For the Kurile-2 event, all stations were equalized to NPNT. Choice of reference stations was based on good SNR. Results of applying the equalization filters are shown in Figures III-2 and III-3.

The first few cycles of the Kamchatka event were better equalized than those of the Kurile event, since the Kamchatka-event P-wave recordings were much more similar in waveform. However, neither event's network similarity was improved enough to indicate that the extra complication of designing and applying equalization filters was worthwhile. Even less improvement would be expected in real-time processing, since average equalization filters would have to be used and a different set of filters for each geological province probably would be required.

Results of processing the two events at the network level using simple beamsteer (BS), signal-to-noise-ratio weighted beamsteer (SNW), and beamsteers of Levinson-equalized data (LE) are shown in Figures III-4 and III-5. All traces except the unprocessed simple beamsteer (which yielded a SNR approximately equal to the average of all station SNR's) were derived from bandlimited data. Indicated improvements in SNR for the bandpass-filtered beamsteer relative to the unprocessed beamsteer are 12.6 and 13.2 db for the Kamchatka and Kurile-2 events, respectively.

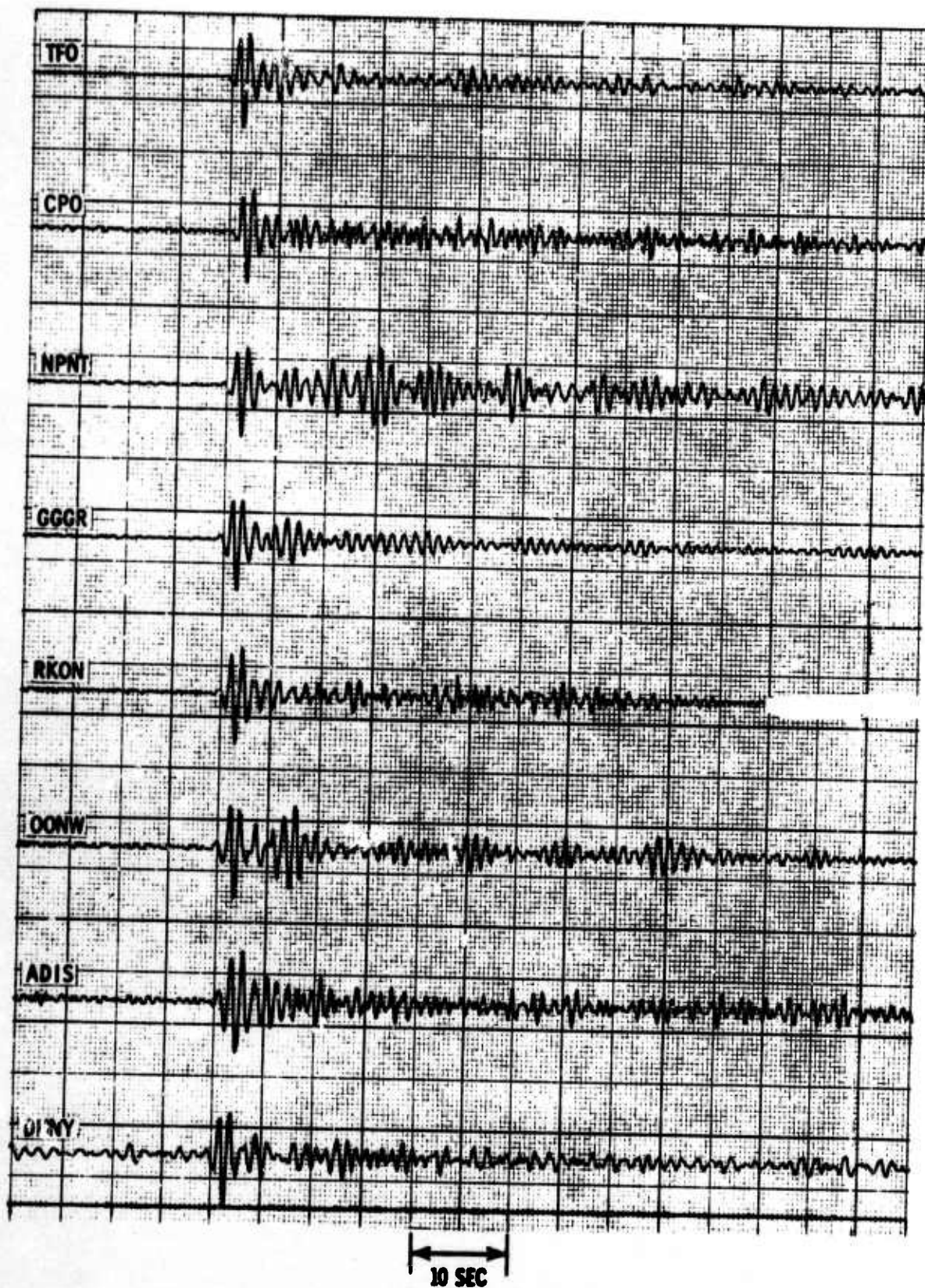


Figure III-2. Levinson-Filtered Equalization of Kamchatka Event to TFO Trace

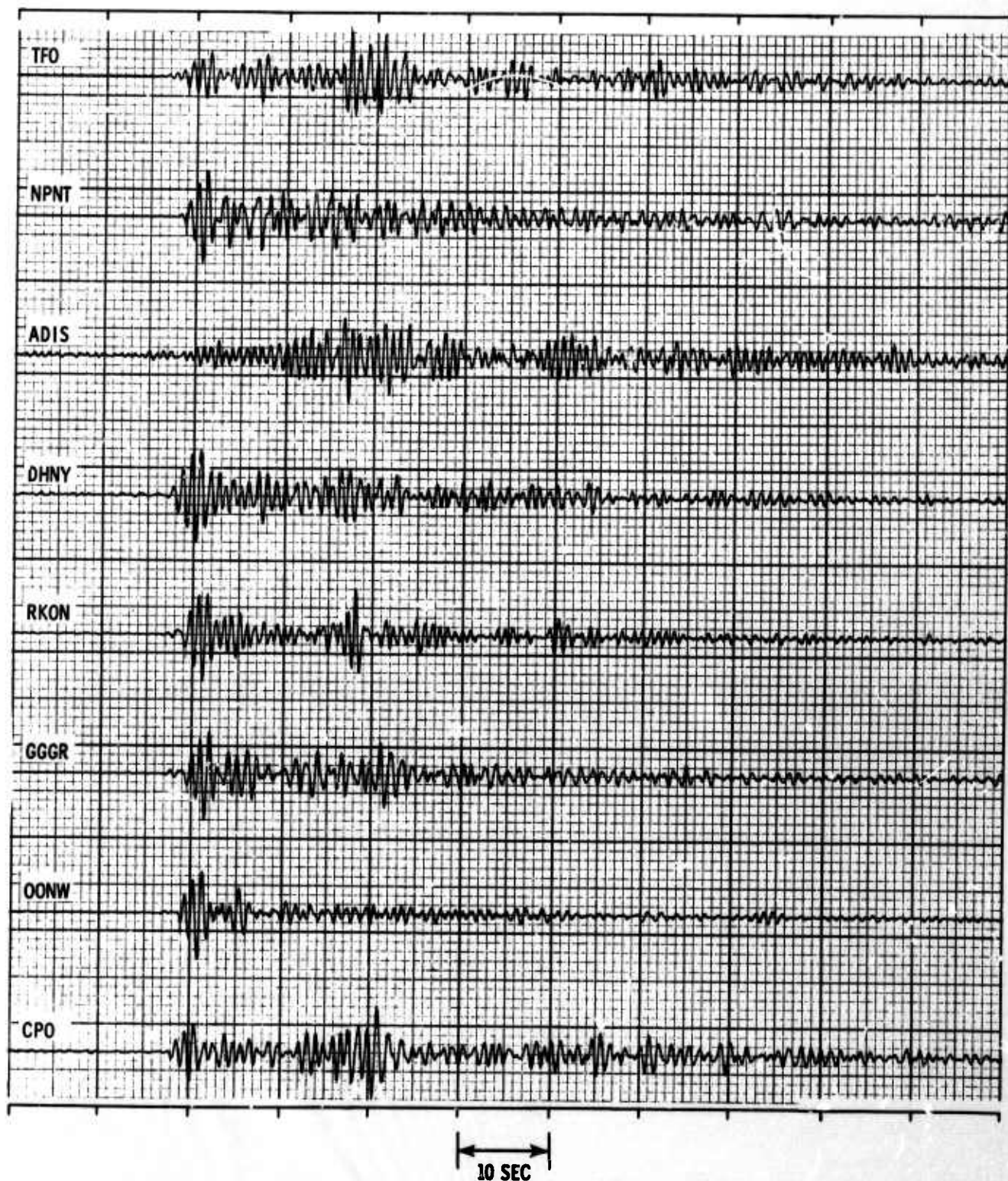


Figure III-3. Levinson-Filtered Equalization of Kurile-2 Event to NPNT Trace

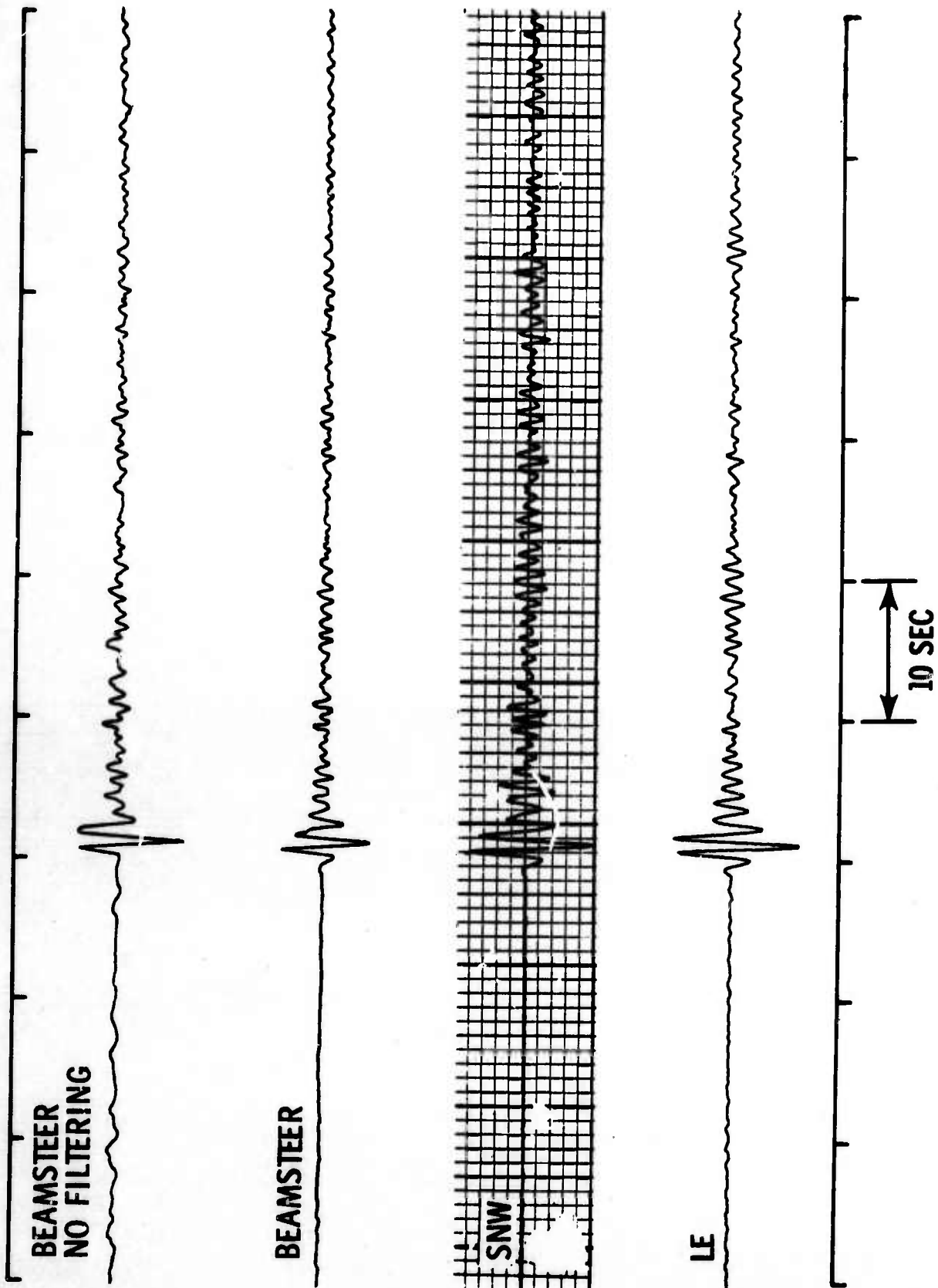


Figure III-4. Kamchatka Event Network Beamsteer Outputs for Four Preprocessing Schemes

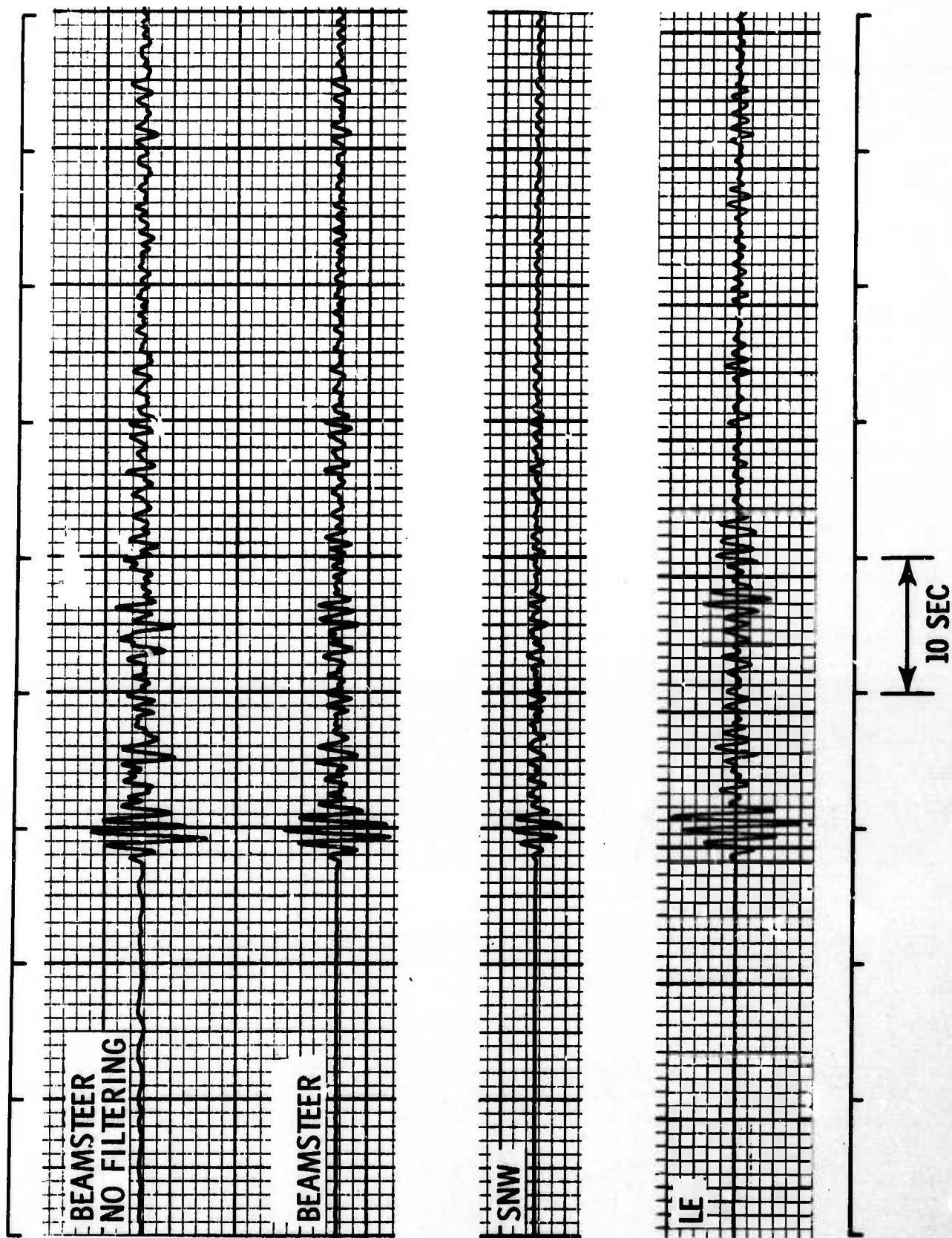


Figure III-5. Kurile-2 Event Network Beamsteer Outputs for Four Preprocessing Schemes



Table III-1 shows the SNR improvements obtained for the bandlimited network-processed outputs relative to the simple bandlimited beamsteer of station outputs. Except when referring to spectral measurements, SNR's are defined as one-half the peak-to-peak signal amplitude divided by the RMS of the noise calculated over a 50-sec gate preceding the signal onset by 5 sec. The performance of the weighted beamsteer is significantly better than beamsteers of either simple bandlimited or Levinson-equalized data.

The performance is better because of the large signal differences from station to station and because increased emphasis is placed on the better signal estimates. It should be pointed out that beamsteers were performed by visual alignments of signals rather than by using the Jeffreys-Bullen traveltimes. Thus, time residuals were compensated for, and the improvements obtained presuppose such corrections.

Table III-1
PEAK SIGNAL-TO-RMS-NOISE-RATIO IMPROVEMENTS FOR
NETWORK-PROCESSING TECHNIQUES
(RELATIVE TO BANDLIMITED BEAMSTEER)

<u>Technique</u>	<u>Kamchatka 1 (db)</u>	<u>Kurile 2 (db)</u>
SNW	+4.2	+7.0
LE	-0.9	+0.6



In Figure III-4, the first two traces are plotted to the same vertical scale; however, the third and fourth traces are scaled up for visual comparison. The SNW output is actually lower in amplitude due to the arbitrary method of weighting: the station output with the largest SNR was multiplied by 1; all other station outputs were multiplied by a scaler less than 1. In Figure III-5, the first three traces are plotted to the same relative scale, while the fourth is scaled differently for plotting.

Power spectra were computed also to compare the effect of the techniques on noise, the primary P-wave, and the coda. Noise power-density spectra N were estimated from the 50 sec of data immediately preceding the P-wave. The P-wave energy-density spectra were estimated by subtracting the noise spectrum N from the spectrum $P' + N'$ obtained for a 50-sec data gate. This data gate consists of the last 45 sec of the data used to estimate N plus the first 5 sec of the P-wave. The spectrum so obtained is an estimate of the true P-wave energy-density spectrum P' .

$$P = P' + N' - N \approx P'$$

The P-coda energy-density spectra C were estimated from the 40 sec of data immediately following the 50 sec of data used to estimate the P-wave spectrum.



To form a basis for measuring signal-to-noise-power improvements as a function of frequency, "average" station spectra were computed by averaging the autocorrelations computed for the various stations. All autocorrelations were Parzen-smoothed before the spectra were computed. The spectra N, P, and C computed for an average station for both events are shown in Figure III-6. Coda power spectrum C in this figure is actually a coda plus noise measurement. The noise power spectrum N shows a rapid drop outside the band passed by the bandpass filter; however, the P and C spectra do not drop to the same level as the N spectra for the very low frequencies (0.0 to 0.5 Hz) and the very high frequencies (3.0 to 4.0 Hz) as might be expected. Probably, this is due to P and C spectra being computed from signals which were truncated, inducing the power shown at the high frequencies. For this reason, the power spectra discussed in this section should be examined only in the 0.8- to 2.8-Hz band.

Figure III-7 compares the effect of beamsteering data from eight stations for both events to an average input trace. Using eight stations, approximately 9-db reduction in noise power is observed, which is approximately equal to a factor of N reduction in power (for N stations). Both events also show a 7- to 9-db reduction in the coda energy, as expected, since large amounts of scattered signal energy appear randomly on the traces and thus are reduced by approximately the same amount as the noise. This scattered signal was reduced very little by station preprocessing because several stations were single-seismometer sites and the array apertures were really too small to reduce the scattered energy effectively. The reduction in coda energy and complexity makes network processing very effective for the estimation of P-wavelet spectral content and P-coda complexity for use in event classification. The small (2 to 3 db) reduction in P energy for the Kamchatka event is not surprising; however, the +2-db value for the P phase of the Kurile event is unexpected. This positive value probably is caused by the definition of P (i. e., $P = P' + N' - N$) and would occur if the noise estimate N were smaller than N'.

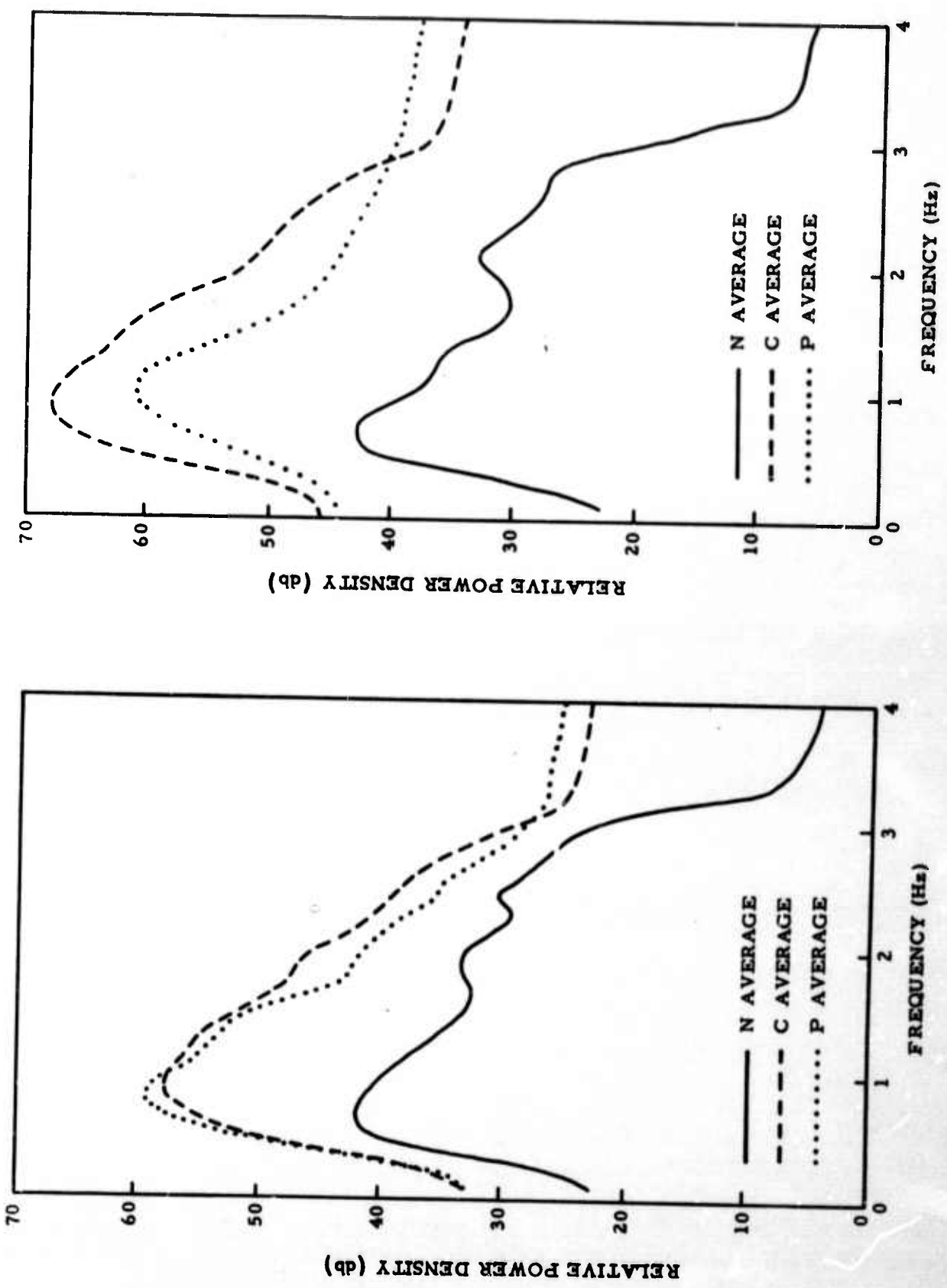


Figure III-6. Kamchatka (left) and Kurile-2 Spectral Ratios Between Average Input Trace and Beamsteer Output Relative to Unity

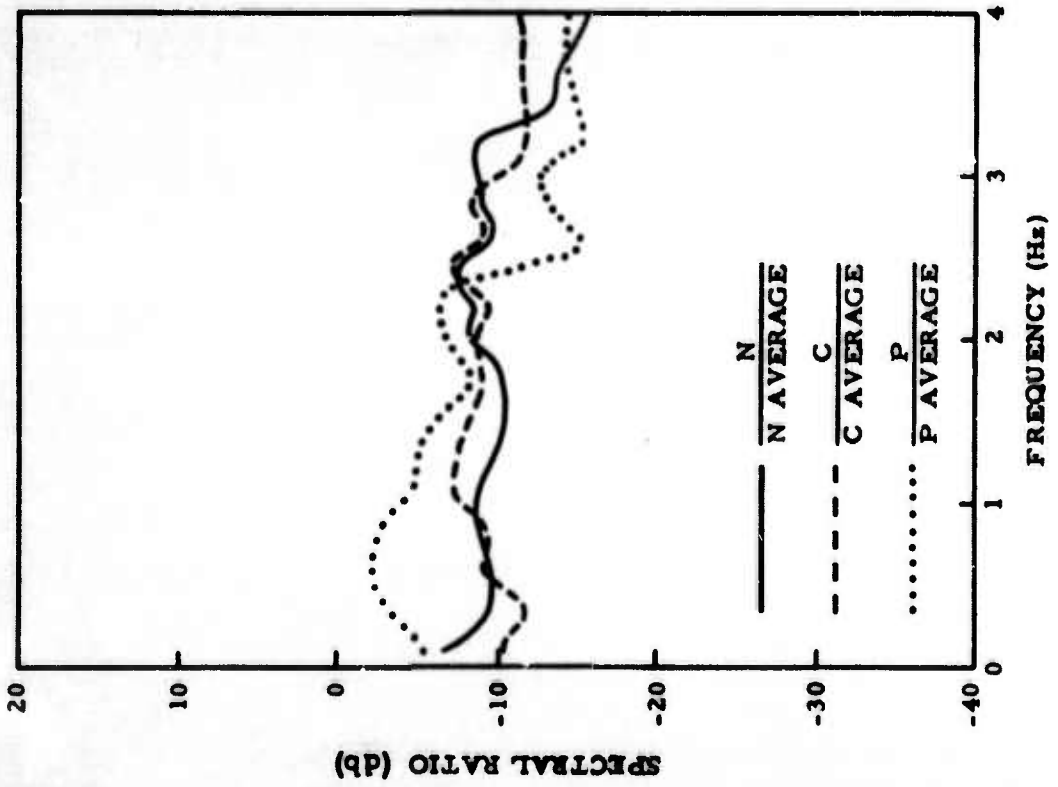
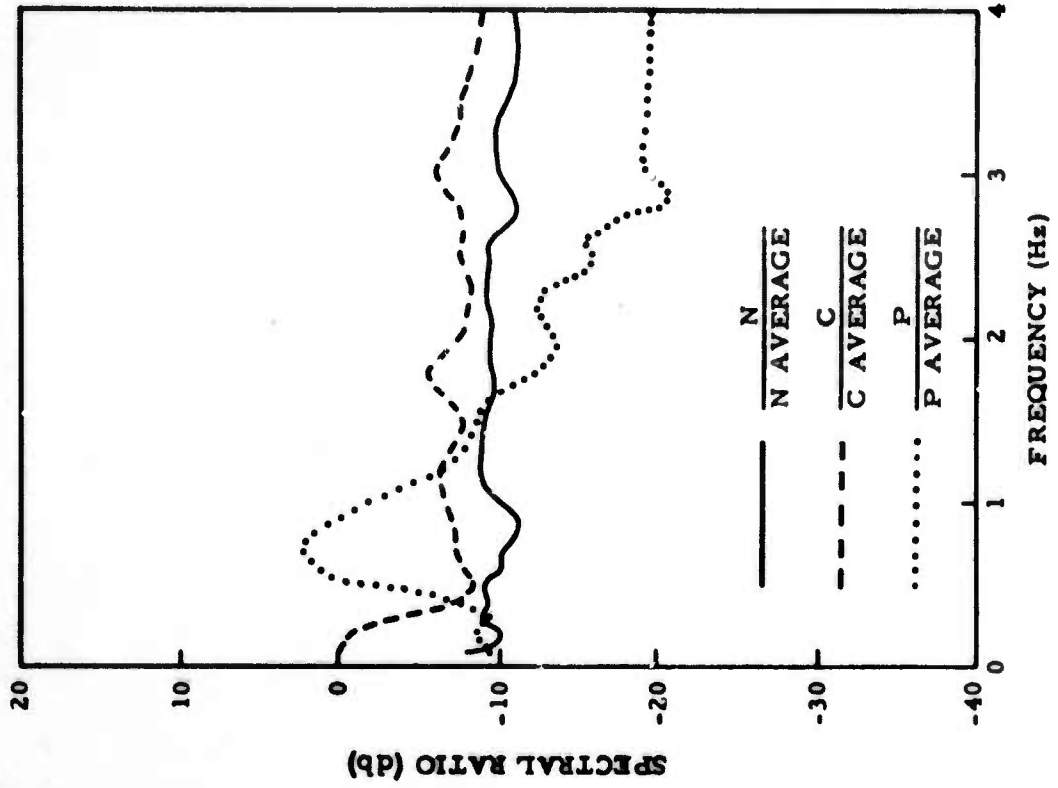


Figure III-7. Kamchatka (left) and Kurile-2 Spectral Ratios for Network Outputs Compared to an Average Input Trace



Figures III-8 and III-9 show the signal-to-noise-power improvements for the various network-processing techniques compared to the average input spectra N_{avg} , P_{avg} , C_{avg} for Kamchatka and Kurile-2 events. As with the previous spectra, only the data between 0.8 and 2.8 Hz should be analyzed. In these figures, the spectra are labeled according to the data used (i. e., noise, P-wave, and coda) and subscripted according to the processing technique used.

In general, Figures III-8 and III-9 show that Levinson equalization produces significant coda rejections throughout the signal band except for the peak signal frequency where little or no rejection occurs. The signal energy scattered at each station adds destructively at the network level; and the Levinson filters, designed only from the initial P phase, act as narrowband filters. SNW produces large improvements in P-wave signal-to-noise power throughout the entire signal band, with very large improvements occurring at the peak signal frequency. For both events, SNW is shown to be the best technique for signal extraction. Simple beamsteering produces fair signal-to-noise-power improvement at peak signal frequencies; but the improvements are less than those for SNW, since weighting proportionately to SNR essentially removes traces with poor SNR from the sum. Neither procedure produces detection results better than the station with the best SNR. Levinson equalization produces results comparable to those for the beamsteer traces with small P-wave improvement but less than those for SNW.

Discussions of Figures III-8 and III-9 are presented on the pages opposite the respective figures.



SUMMARY OF FIGURE III-8

$$\frac{C_{le}/N_{le}}{C/N}$$

Levinson equalization (LE) produces significant rejection of coda energy throughout the signal band of 0.8 to 2.0 Hz except at the peak signal frequency of 1.0 Hz. This suggests either that the bulk of this energy is scattered signal or that it differs in frequency from the P-wave.

$$\frac{P_{snw}/N_{snw}}{P_{avg}/N_{avg}}$$

Signal-to-noise-ratio weighting (SNW) produces signal-to-noise-power improvements of 3 to 12 db throughout the signal band, with improvements of 12 db at the peak signal frequency.

$$\frac{P/N}{P_{avg}/N_{avg}}$$

Beamsteering (BS) produces 3- to 7-db improvement in the signal band; however, the improvements are approximately 6 db less than that obtained by weighted beamsteering (SNW) at the peak signal frequency.

$$\frac{P_{le}/N_{le}}{P_{avg}/N_{avg}}$$

Levinson equalization produces 3- to 8-db improvement in signal-to-noise power throughout the signal band, with approximately 5-db improvement at the peak signal frequency. This improvement is not significantly more than that obtained by simple beamsteering and is well below that obtained with SNW.

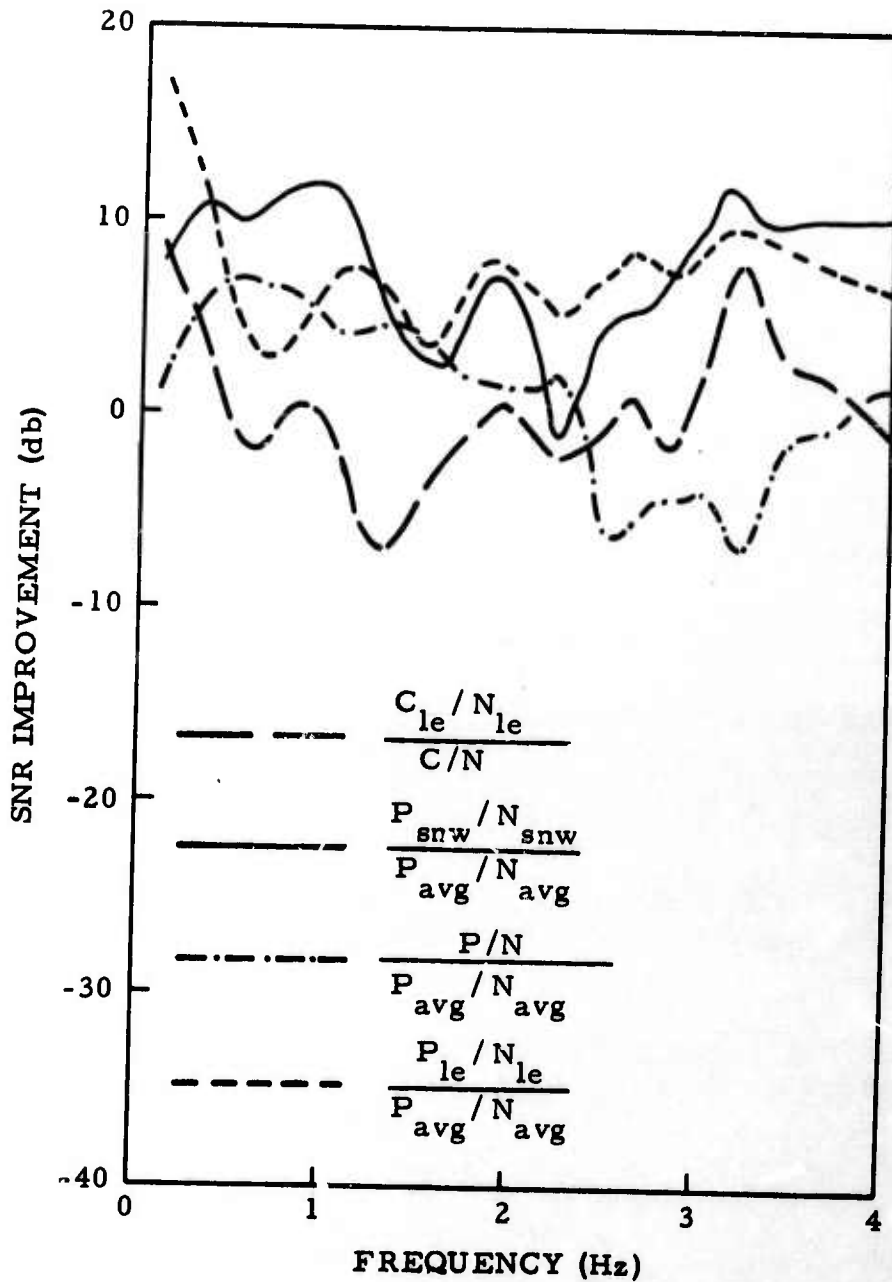


Figure III-8. Kamchatka Signal-to-Noise-Ratio (SNR) Improvements for Network Processing



SUMMARY OF FIGURE III-9

$$\frac{C_{le}/N_{le}}{C/N}$$

Levinson equalization produces coda rejection of 1 to 8 db throughout the signal band, with small rejections occurring at the peak signal frequency. Again, this represents either reduction in scattered signal or phase attenuation due to the Levinson-filter response which is peaked for the P-wave.

$$\frac{P_{snw}/N_{snw}}{P_{avg}/N_{avg}}$$

This technique produces extremely high SNR improvements of 6 to 18 db. The reason for the extremely high values, much larger than N, is that the SNR's of the various input traces are extremely different.

$$\frac{P/N}{P_{avg}/N_{avg}}$$

Beamsteering of network data produces good SNR improvements throughout the frequency band, with maximum improvement of 13 db at the peak signal frequency. However, the improvements are less than those for SNW for all traces.

$$\frac{P_{le}/N_{le}}{P_{avg}/N_{avg}}$$

Levinson equalization produces 0- to 10-db improvement in signal-to-noise power, with the 10-db improvement occurring approximately at the peak signal frequency. However, as with the simple beamsteer, the improvements are smaller than those for SNW.

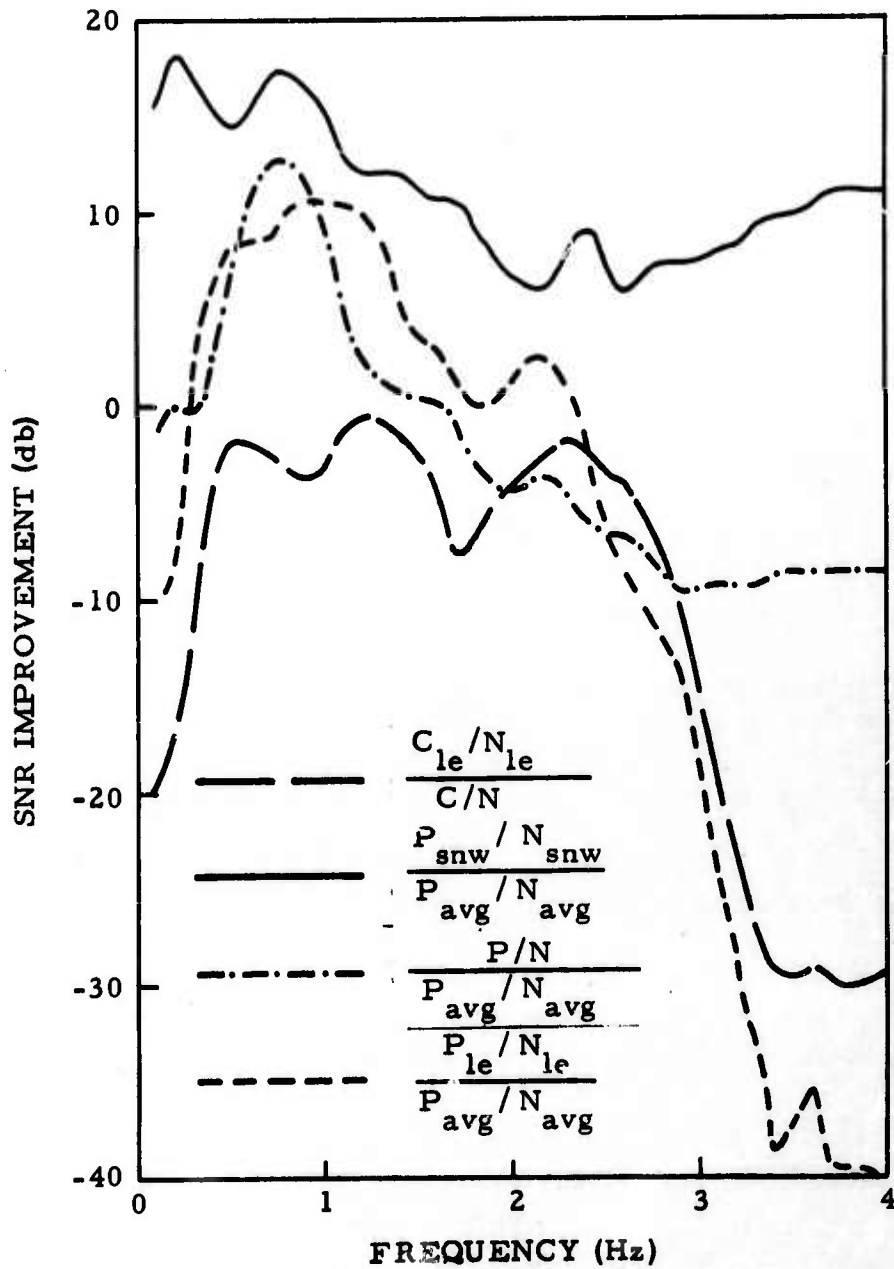


Figure III-9. Kurile-2 Signal-to-Noise-Ratio (SNR) Improvements for Network Processing



In summary, this study shows that network processing should be a useful technique for obtaining improved signal estimates which should, in turn, influence event classification procedures. Signal extraction is demonstrated feasible at the network level, even with events reflecting rather complex radiation patterns. Improvements with the different techniques undoubtedly vary among events; but as shown in both the peak-signal-to-RMS-noise measurements and the spectral analysis, SNR-weighted beamsteering bandpass-filtering is consistently a better extraction processing technique. When compared to the other processing methods, this technique shows additional improvements at the frequency of peak signal energy — from 7 to 13 db for the Kamchatka event and 4 to 18 db for the Kurile event.

Levinson-equalization-filtering results indicate that some improvement in signal waveform similarity can be gained by designing and applying filters for each specific event. However, the limited improvements do not seem to justify the required increase in processing complexity.

The reduction in the coda energy is an important result of this study, since event classification is greatly benefited by improved estimates of P-coda complexity and relative spectral content.

Results of this study show promise for significant improvements in location of signal epicenters and classification of sources through postdetection network processing. For on-line processing, the SNW technique could be extremely valuable. A series of relative signal weights for each area to be monitored could be learned quickly, and RMS noise could be monitored continuously at each station so that the proper weights for weighted beamsteering to any location would always be known. Since beamsteers were accomplished by visual trace alignment, adjustments for time residuals were made automatically, and the rather significant influence that such residuals would undoubtedly exert on processing procedures was not evaluated. However, it is believed that with expected improvements in epicentral location, the time residual problem can be solved at the network level through compilation of average regional residuals.



SECTION IV

PHASE EXTRACTION STUDY

One means of positively identifying an earthquake event is simply detecting and confirming depth phases which indicate a focal depth greater than any possible underground explosion. Therefore, one important aspect of network processing to be investigated is its ability to reject noise and scattered P-wave energy, thereby enhancing depth phases. This section presents results of an initial investigation of various network-processing techniques for the enhancement of depth phases.

Large amounts of scattered signal energy, which cannot be rejected completely at the array level, will appear as random energy at the network level. Therefore, a network of N seismic stations should be able to achieve approximately a \sqrt{N} reduction in the amplitude of this scattered signal energy.

Depth phases might be enhanced by beamsteering the network so as to enhance the pP phase if the event hypocenter were known. But this method requires prior knowledge of the focal depth which is just the information being sought. Fortunately, the time shifts required may be obtained from only a knowledge of the approximate epicenter. The pP-P time interval is naturally a rapidly varying function of focal depth. However, the difference between the pP-P interval at one station and the pP-P interval at another station is primarily a function of the relative distances of the stations from the epicenter and varies slowly with focal depth. This difference of pP-P intervals is the information required, and it varies slowly with epicentral distance difference so that even the epicenter need not be known exactly. If an intermediate depth, say 33 km, were assumed and the network were beamsteered on that basis, all pP phases would be within a fraction of a second in phase (assuming the same polarity for pP at all stations).



Traveltime anomalies are quite naturally a serious obstacle to effective beamsteering. When beamsteering for pP, however, a large part of the time anomaly (that arising from differences in the mantle and crust beneath the various stations) can be avoided. If the P-wavelet is used as a matched filter at each station and the outputs (previously designated as P-30 correlations*) are time-shifted and summed on the basis of the pP-P time interval expected for each station, that part of the time anomaly cancels out. Some time anomalies may still exist, however, due to inhomogeneities in the crust above the event hypocenter. For this reason and also because the pP-phase polarity relative to the P-phase polarity may not be the same at all stations, the P-30 correlations are smoothed before summing. Usually, smoothing is accomplished by squaring or rectifying each P-30 correlation then convolving it with a short (1 to 2 sec) Danielle function.

An experiment was performed evaluating the ability of a limited network to enhance depth phases while rejecting scattered signal energy. Only a small number of events were processed in this initial investigation, and those processed did not contain good evidence of depth phases.

The P-30 correlation was used to detect depth phases. The P-phase wavelet used in this study was 5 sec long. Correlation of this function with the original time trace included at least 35 sec of P-coda and 30 sec of noise preceding the P onset. All P-30 correlations were smoothed by squaring and then integrating over a 2.5-sec gate.

The four events processed in this experiment were discussed in Section II with the events shown in Figures II-1 through II-4 and described in Table II-1.

* Texas Instruments Incorporated, 1966: Study of Statistical Discrimination between Earthquakes and Explosions, Annual Rpt. No. 1, Contract AF 19(628)-4173, 30 Apr.



For each event, P-30 correlations of station outputs (not band-limited) were computed, normalized by dividing by the total power in the correlating wavelet, and then squared and integrated using a 2.5-sec integration interval. In addition, the station outputs for the Kurile events were squared and integrated, also with a 2.5-sec integration gate.

The P-30 correlations and the smoothed correlations for the Kamchatka event are shown in Figures IV-1 and IV-2, respectively, with arrows indicating times at which depth phases would be expected, based on the USC&GS reported depth. These figures also show the result of time-aligning and stacking the subarray outputs by the pP-P time differences based upon traveltimes in the Jeffreys-Bullen tables for the reported depth. Since the P-30 correlations were normalized before summing, each subarray was given an equal weight. The horizontal scales in the figures show time in seconds relative to the arrival of the P phase for the station outputs. For the averages, which are aligned to enhance pP, the reference point (0) is the expected time of arrival of this phase.

The individual-station P-30 correlations show that differences in pP travel paths through the crust above the event hypocenter produce differences between observed phase arrival times and theoretical arrival times. These variations produced a smearing of the pP phase in the P-30 correlation stack. However, most noise and scattered energy in the 3 to 4 sec preceding the phase was cancelled. The pP phase was not as apparent on the squared and integrated trace, since this process responds to changes in power and is not affected by the change in frequency from the scattered energy and noise in the coda to the pP onset.

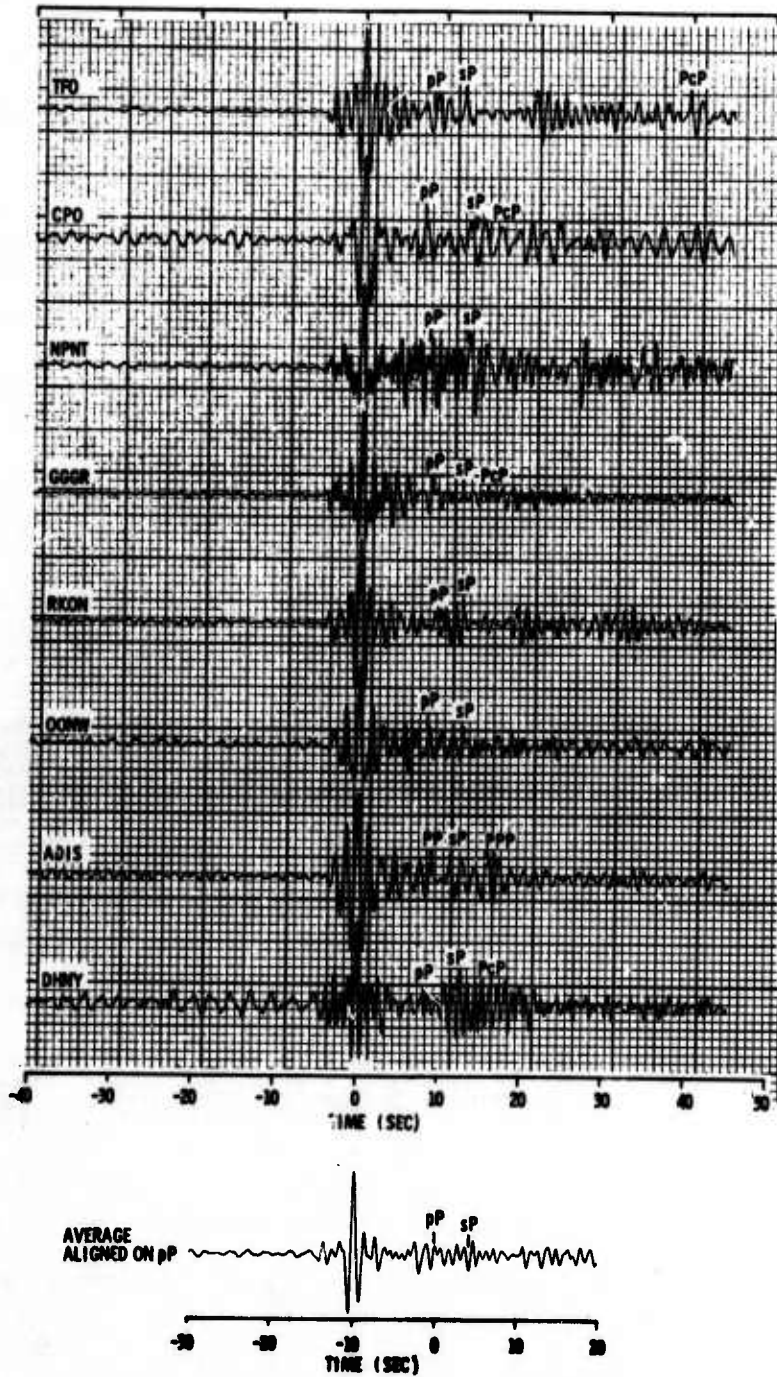


Figure IV-1. Kamchatka P-30 Correlations and Average Aligned on USC&GS pP

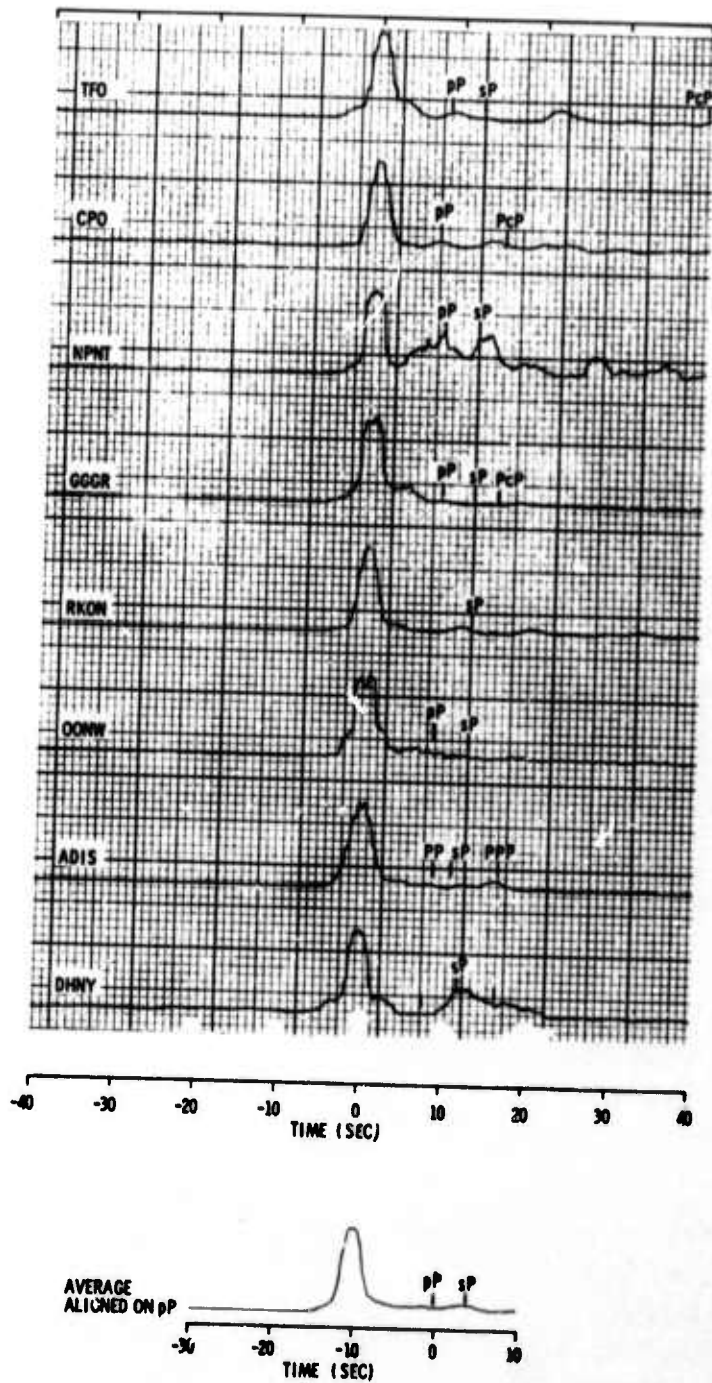


Figure IV-2. Kamchatka Smoothed P-30 Correlations and Average Aligned on USC&GS pP



The P-30 correlations for the Kurile-1 event are shown in Figure IV-3 and the corresponding smoothed correlations in Figure IV-4. The smoothed time traces and the worldwide sums for each process are shown in Figure IV-5, with the USC&GS times for pP and PcP included. Indication of pP arrivals can be seen at NPNT, ADIS, and to a lesser degree at OONW. A possible explanation for pP showing only on these traces is that the source mechanism for this event was such that radiation of pP was focused through the north polar region. The smoothed P-30 correlations showed no improvement over the unsmoothed P-30 correlations for this event. Some additional phases are weakly indicated on the individual station outputs, but they are not indicated on the network output. The phase PcP can be seen on the traces for RKON, GGGR, and OONW. PcP for the other stations arrives either too close to P to be resolved or too much later to be included in the P-30 correlation.

Figures IV-6 and IV-7 show the P-30 correlations and smoothed P-30 correlations, respectively, for the Kurile-2 event, with times indicated for the pP, PcP, P, and sP phases corresponding to a depth of 65 km.

The average trace shown in the figures was the result of aligning to enhance a pP phase corresponding to the USC&GS reported depth of 33 km. The peak corresponding to the actual pP phase is seen much later than the expected arrival time, indicating a depth greater than 33 km. The 65-km depth was estimated by measuring the arrival-time difference between the observed pP peak and the P onset. There is evidence of a pP phase corresponding to a depth of 65 km at all stations except NPNT, where pP appears to occur early.

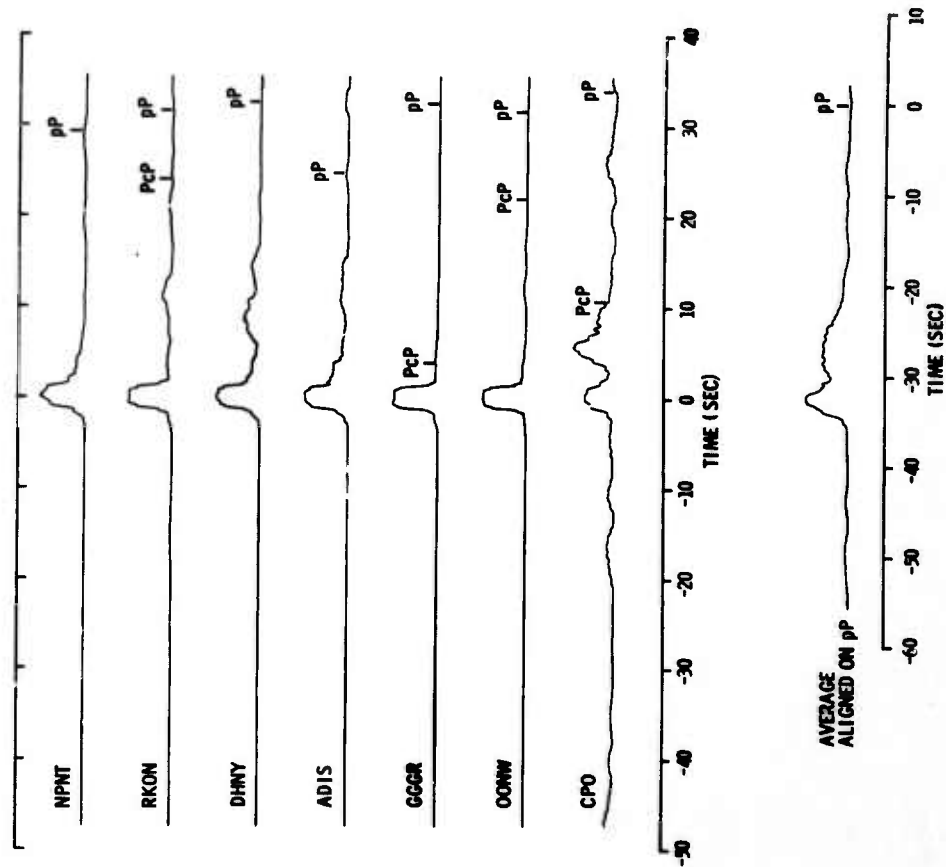


Figure IV-4. Kurile-1 Smoothed P-30 Correlations and Average Aligned on USC&GS pP

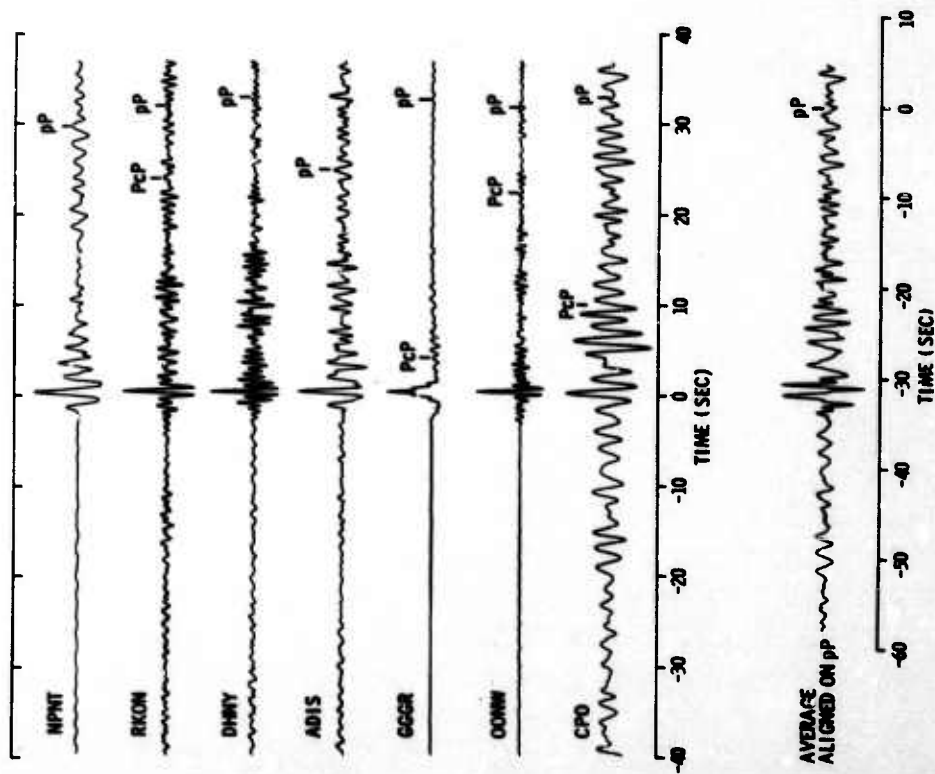


Figure IV-3. Kurile-1 P-30 Correlations and Average Aligned on USC&GS pP

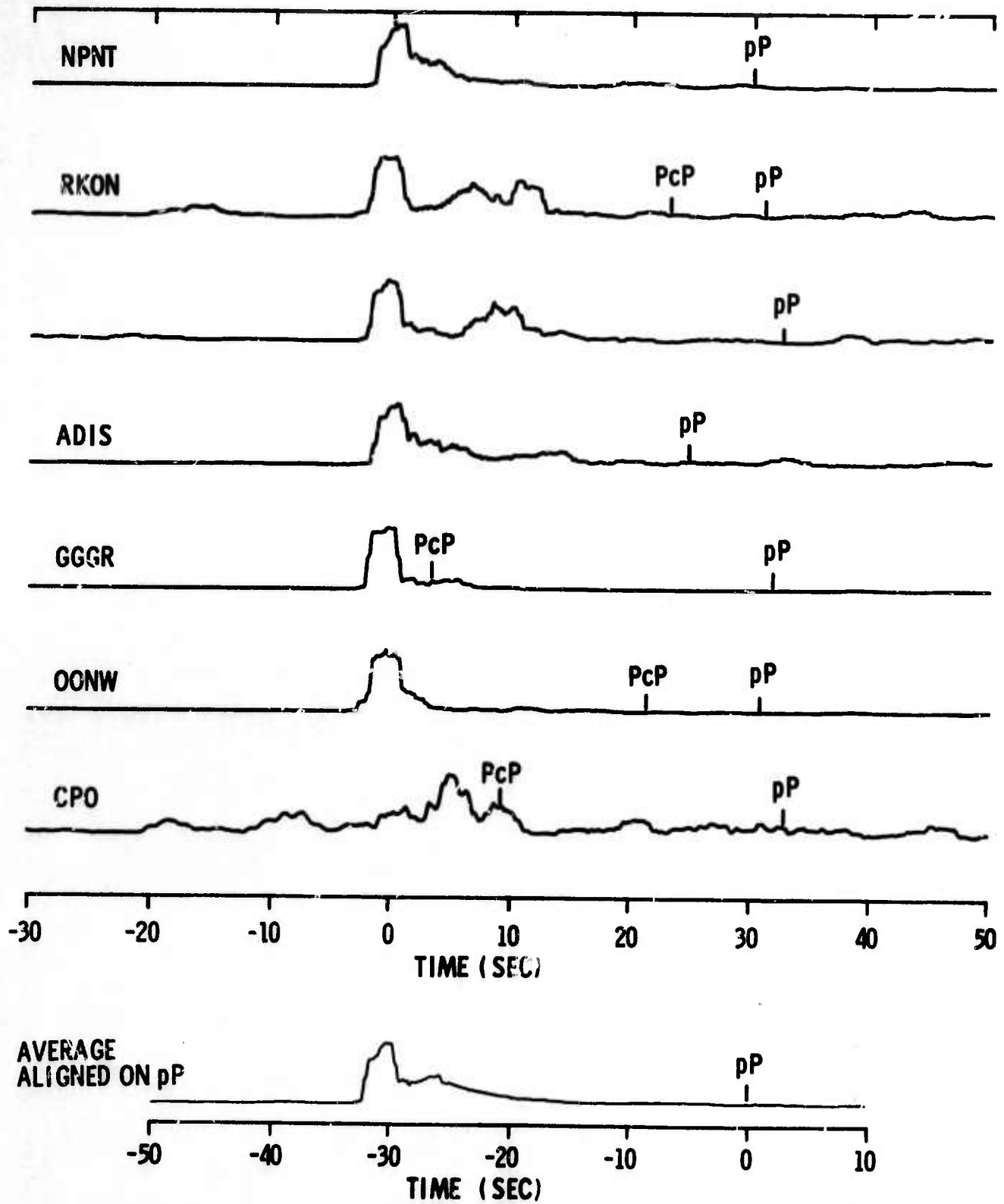


Figure IV-5. Kurile-1 Smoothed Time Traces and Average Aligned on USC&GS pP

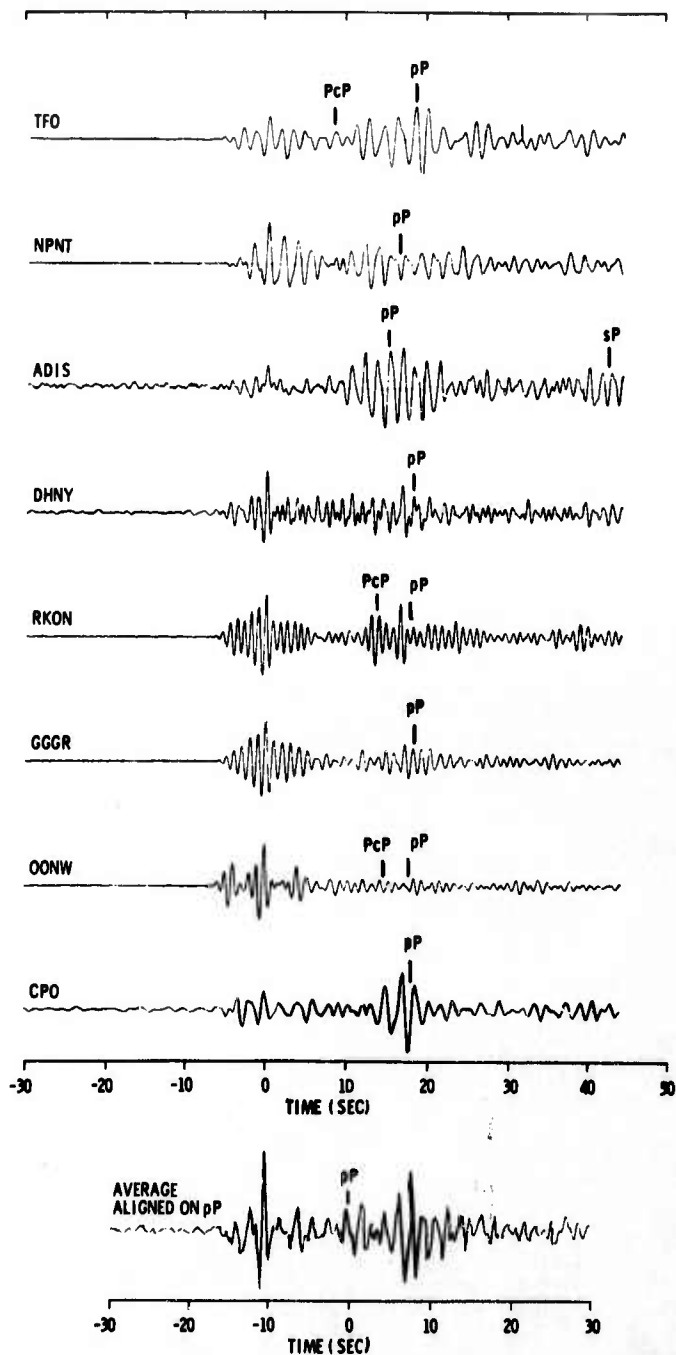


Figure IV-6. Kurile-2 P-30 Correlations and Average Aligned on USC&GS pP

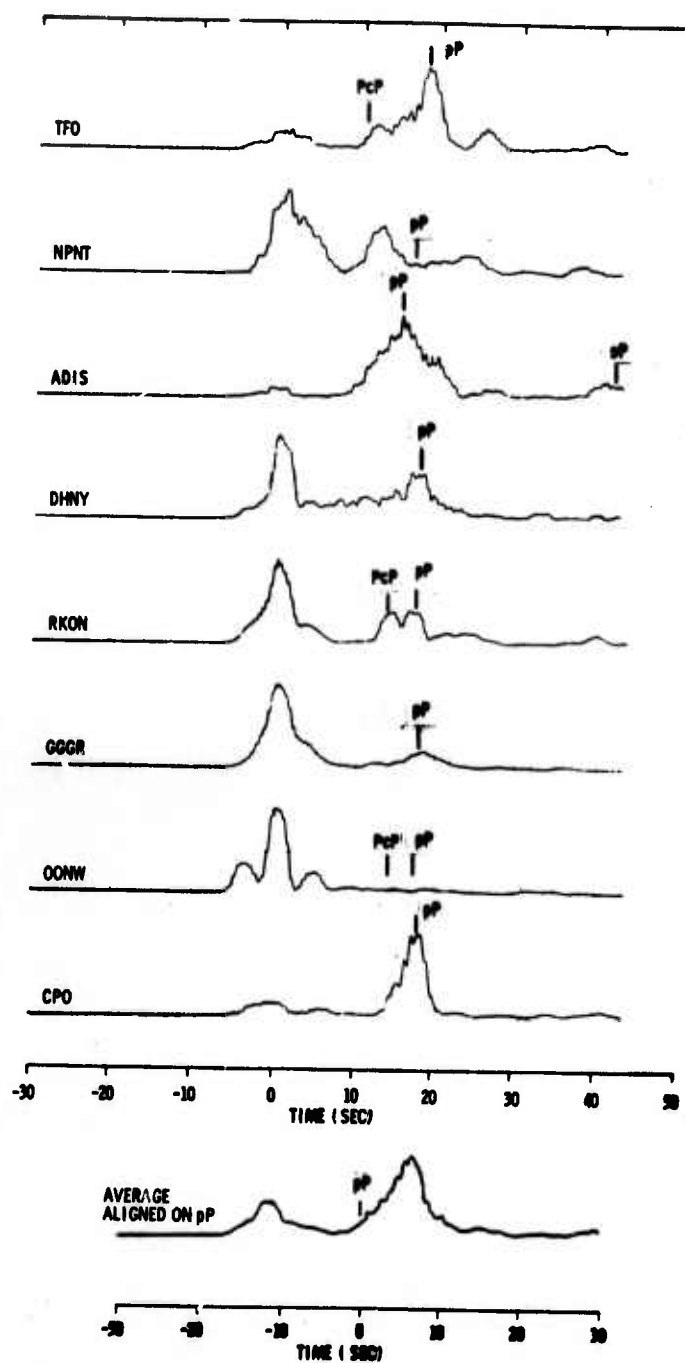


Figure IV-7. Kurile-2 Smoothed P-30 Correlations and Average Aligned on USC&GS pP



The average of the smoothed time traces shows two distinct peaks (Figure IV-8). The two peaks are consolidated into one peak by the P-30 correlation stacks. This is believed to be primarily a misalignment problem in the time traces rather than evidence of two distinct phases. Time-shifting to align the pP phase was done after having visually aligned the P phases. Some P-phase misalignment is probable and is reflected in the alignment for pP when pP-P time shifts are introduced. The P-30 correlation is not so sensitive to these residuals, since it only requires that the P-wave be contained within the 5.0-sec wavelet. Thus, the relative timing between P and pP is preserved by the correlation operations.

The Kurile-3 event P-30 correlations and smoothed P-30 correlations are shown in Figures IV-9 and IV-10, respectively; and the smoothed time traces are shown in Figure IV-11. The USC&GS expected arrivals for phases occurring in this interval are indicated again. The LZBV array, 137.8° from the epicenter, did not record a P phase; however, the phases PKP and pPKP are plainly visible. Indications of the presence of pP can be seen 2 to 3 sec ahead of the expected arrival times for TFO, CPO, ADIS, and GGGR subarrays, indicating that the depth was shallower than the 60 km reported. Summation of the P-30 correlations enhanced the peak due to the pP phase. Smoothed P-30 correlation sums and the smoothed time-trace sums showed better resolution of pP, since phase polarity does not affect the sum. However, the network-processed trace shows evidence of a depth phase, while some of the individual array traces show no sign of depth phases. Therefore, network processing would correctly classify this event as an earthquake, while independent use of the various arrays might produce ambiguous event identification.

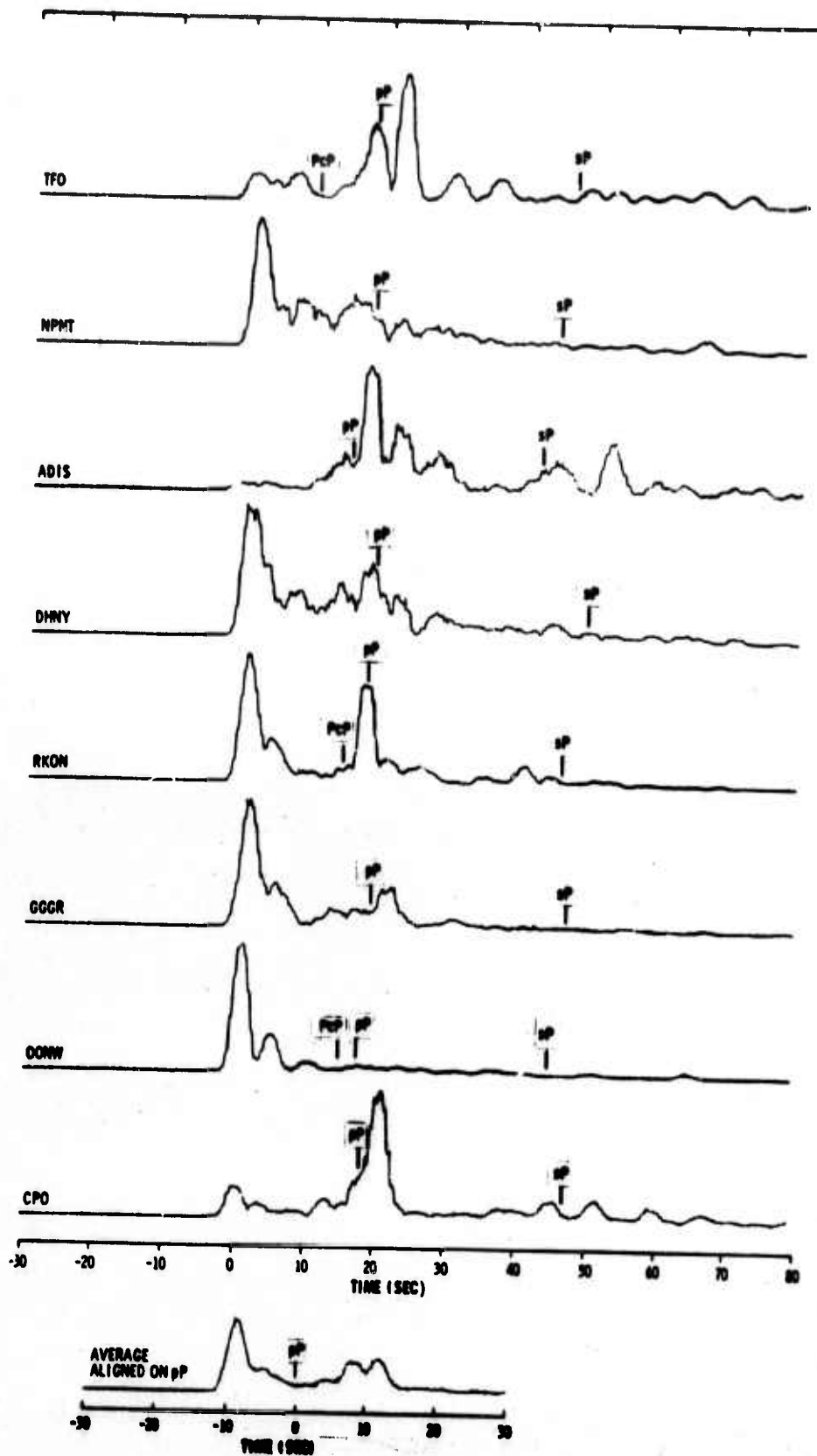


Figure IV-8. Kurile-2 Smoothed Time Traces and Average Aligned on USC&GS pP

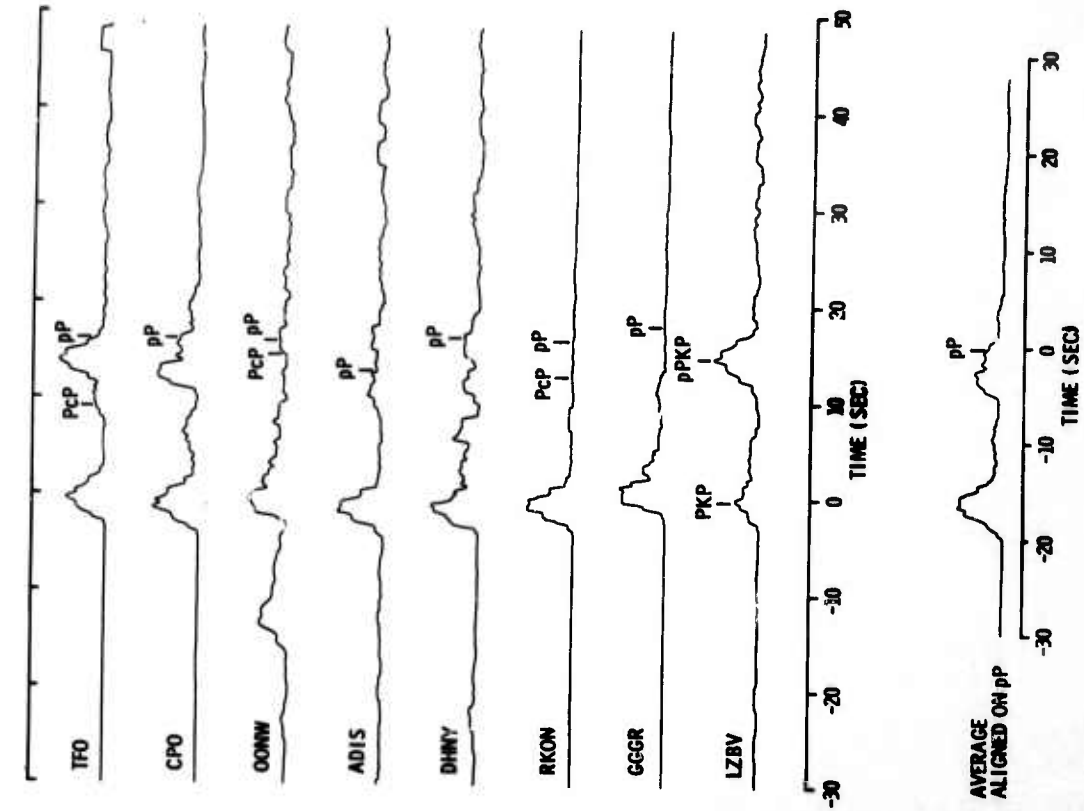


Figure IV-9. Kurile-3 P-30 Correlations and Average Aligned on USC&GS pP

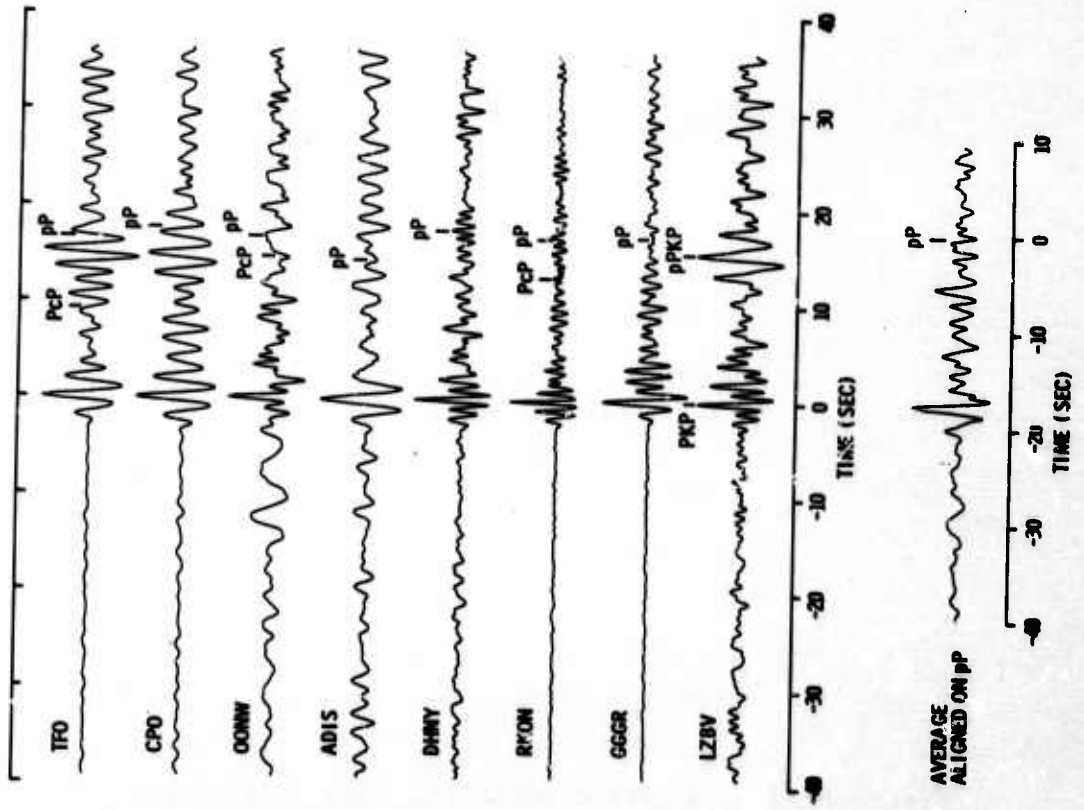


Figure IV-10. Kurile-3 Smoothed P-30 Correlations and Average Aligned on USC&GS pP

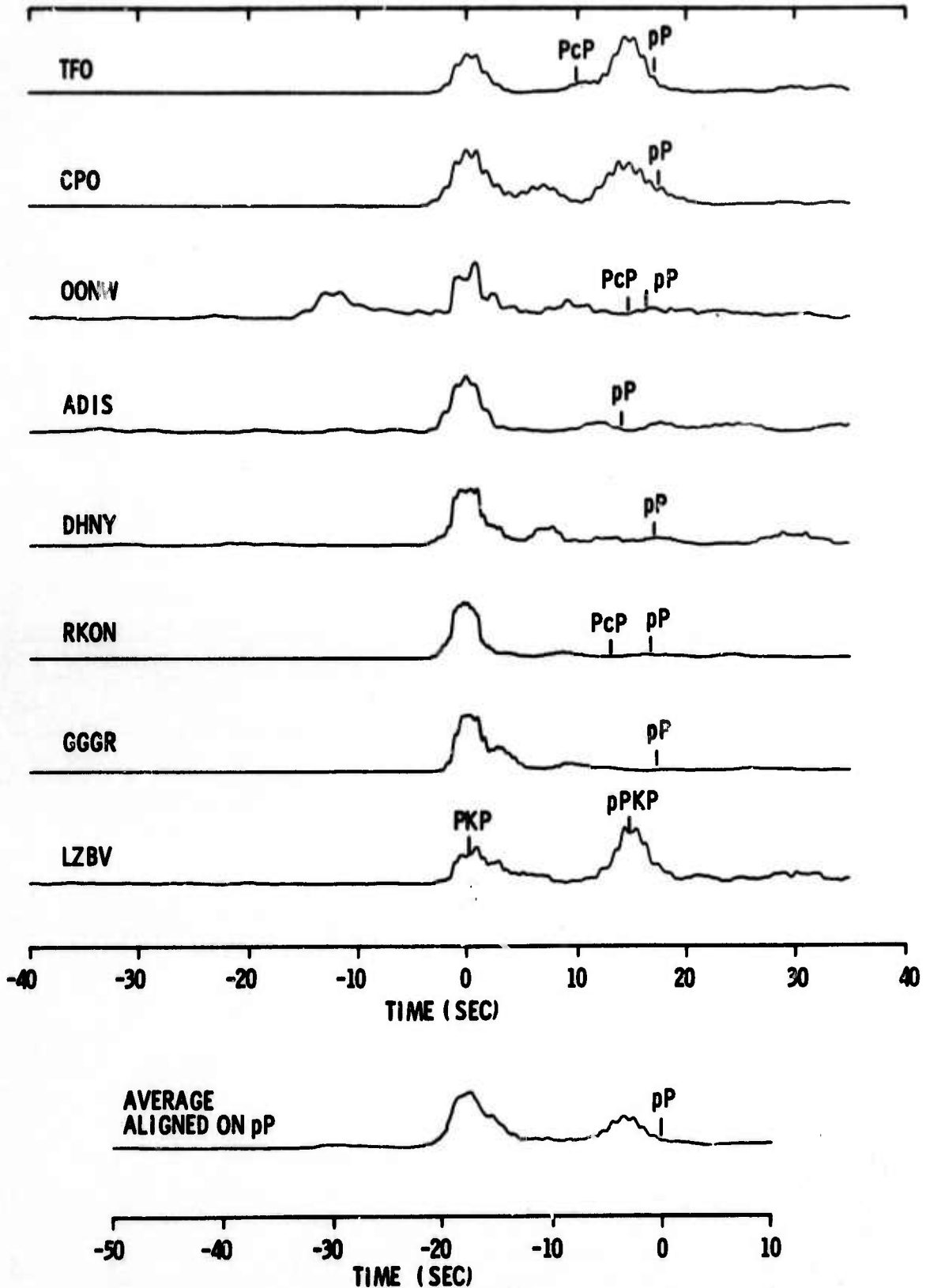


Figure IV-11. Kurile-3 Smoothed Time Traces and Average Aligned on USC&GS pP



In summary, network processing for depth-phase extraction continues to appear promising. While results obtained with the rather inadequate network used for this study are only moderately successful, it appears quite obvious that a network consisting of a greater number of stations and representing more comprehensive coverage would significantly improve the capability for depth-phase detection. Even the present network illustrates the ability to resolve ambiguities arising from station-to-station differences in depth-phase readability.

BLANK PAGE



SECTION V

SIGNAL SEPARATION STUDY

The detection of weak events in the presence of stronger events is important in seismic event classification, since an explosion could be masked by a large earthquake occurring before and in the same geographic region as the explosion. To study the ability of a limited network to resolve seismic events occurring close together in space and time, an experiment using square-and-integration of network beamsteer output traces was performed with two time-overlapping events. This technique is very effective for monitoring small areas of interest but is clearly impractical as a means of continuously monitoring all seismic regions of the earth. An area of interest, however, might be defined as the time and epicentral region of a previously detected event so that detailed examination of all events of interest is practical.

Four synthetic records of time-overlapping events and one recording containing a single event were used in the study. The overlapping event records were constructed from the short-period recordings of the Kamchatka event P-wave at the eight stations (Figure II-1) and the P-wave of the more complex earthquake Kurile 2 as recorded at the GGGR station. The single-station recording of the complex earthquake was added to each of the eight station recordings of the simple earthquake to simulate time-overlapping events. The complex trace was scaled to have the same relative power between stations as the recordings of the simple event. Variations in origin-time differences and magnitude differences allowed construction of four different overlapping event records. The events simulated were



- Case A — A single event
- Case B — A simple event and a complex event, both of the same magnitude, occurring at the same time with epicenters 1° apart
- Case C — Same as Case B except the simple-event magnitude is one-half magnitude unit less than that of the complex event
- Case D — A simple event occurring 10 sec after a complex event of equal magnitude, with epicenters 1° apart
- Case E — Same as Case D except the simple-event magnitude is one-half magnitude unit less than that of the complex event

Traveltimes taken from the Jeffreys-Bullen tables were used to construct the 8-station records for each case investigated. Station time residuals were assumed to be 0.

For each case, the 8-station records were beamsteered to each point on a $2^\circ \times 2^\circ$ grid covering the epicenter area. The grid was divided into 0.5° increments of latitude and longitude and encompassed the area 53.3°N to 55.3°N and 160.7°E to 162.7°E . In each case, the simple-event epicenter was at 54.8°N , 161.7°E and the complex event at 53.8°N , 161.7°E .

For each of the five cases, 25 beamsteered traces (one for each location on the $2^\circ \times 2^\circ$ grid) were formed, squared, and integrated using a 2.5-sec integration gate. The values of the traces so obtained at five different time intervals were then converted to decibels (referenced to the maximum of the 625 values), and beamsteer plots contoured in decibels were developed. The beamsteer plots show relative power for each location on the grid at each time interval.



Figures V-1 through V-5 present the 8-station records for the five cases being studied. (Figure V-2 also shows the GGGR recording of the Kurile event.) Figures V-6 through V-10 show the 25 beamsteered traces for each case. At the top of each figure, numbered arrows indicate the times corresponding to the center of the 2.5-sec integration gates where the beamsteer plots were formed. For each case, the plots have numbers corresponding to the numbered arrows. It should be noted that the time gates are not evenly spaced and actually overlap in certain cases.

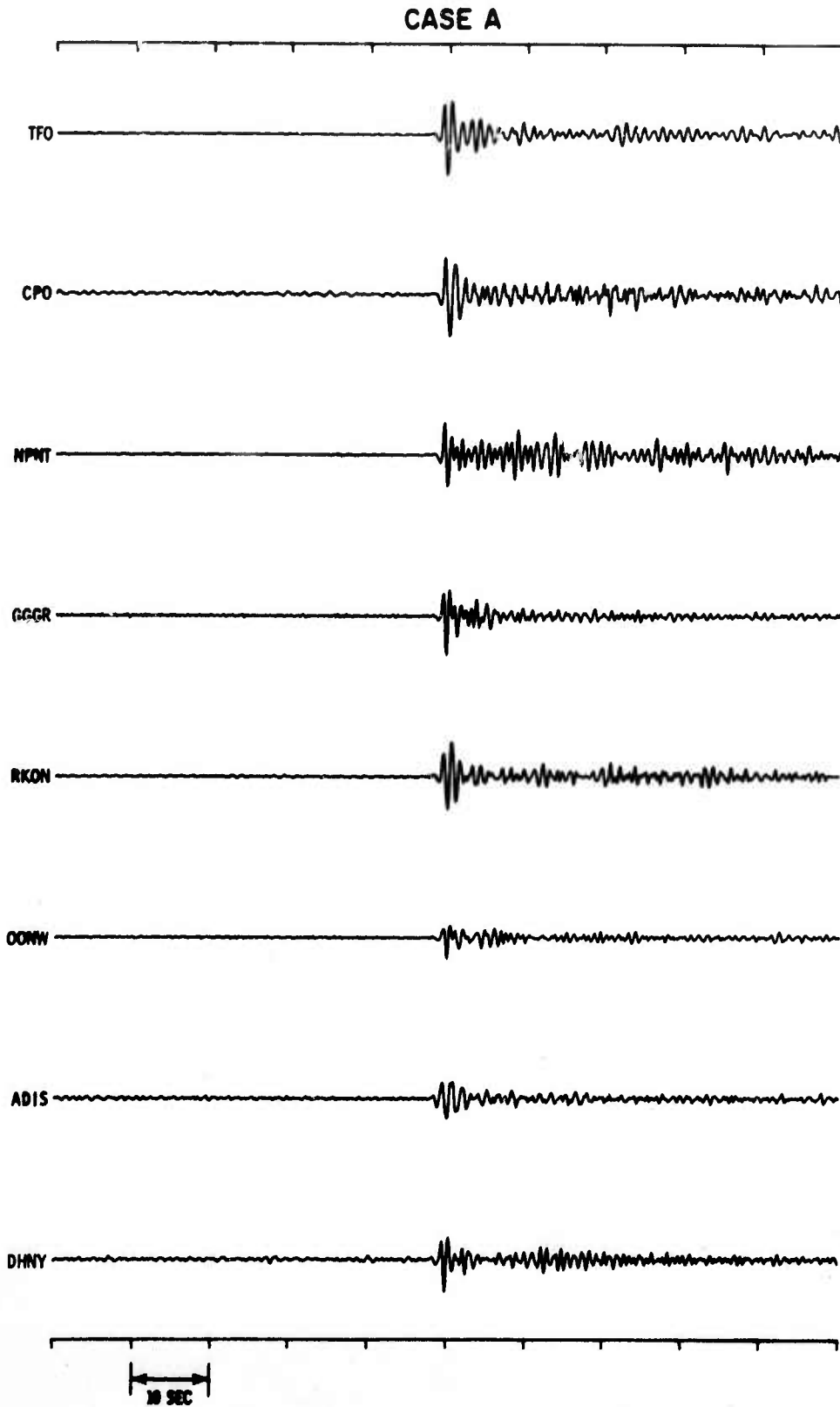


Figure V-1. Case A — 8-Station Recordings of 5.8-Magnitude Earthquakes

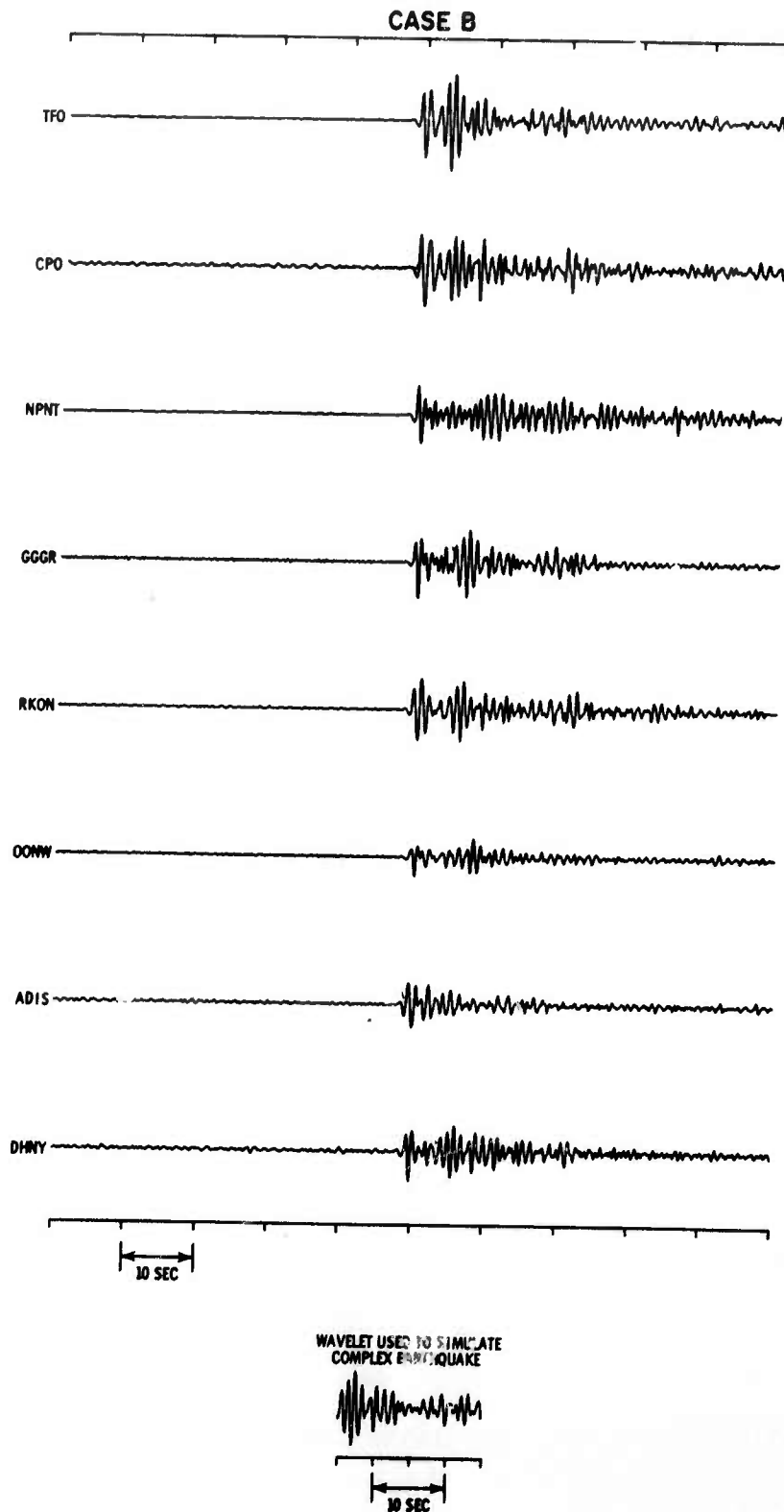


Figure V-2. Case B — Simulated 8-Station Recording of Two 5.8-Magnitude Earthquakes Occurring Simultaneously and 1° Apart

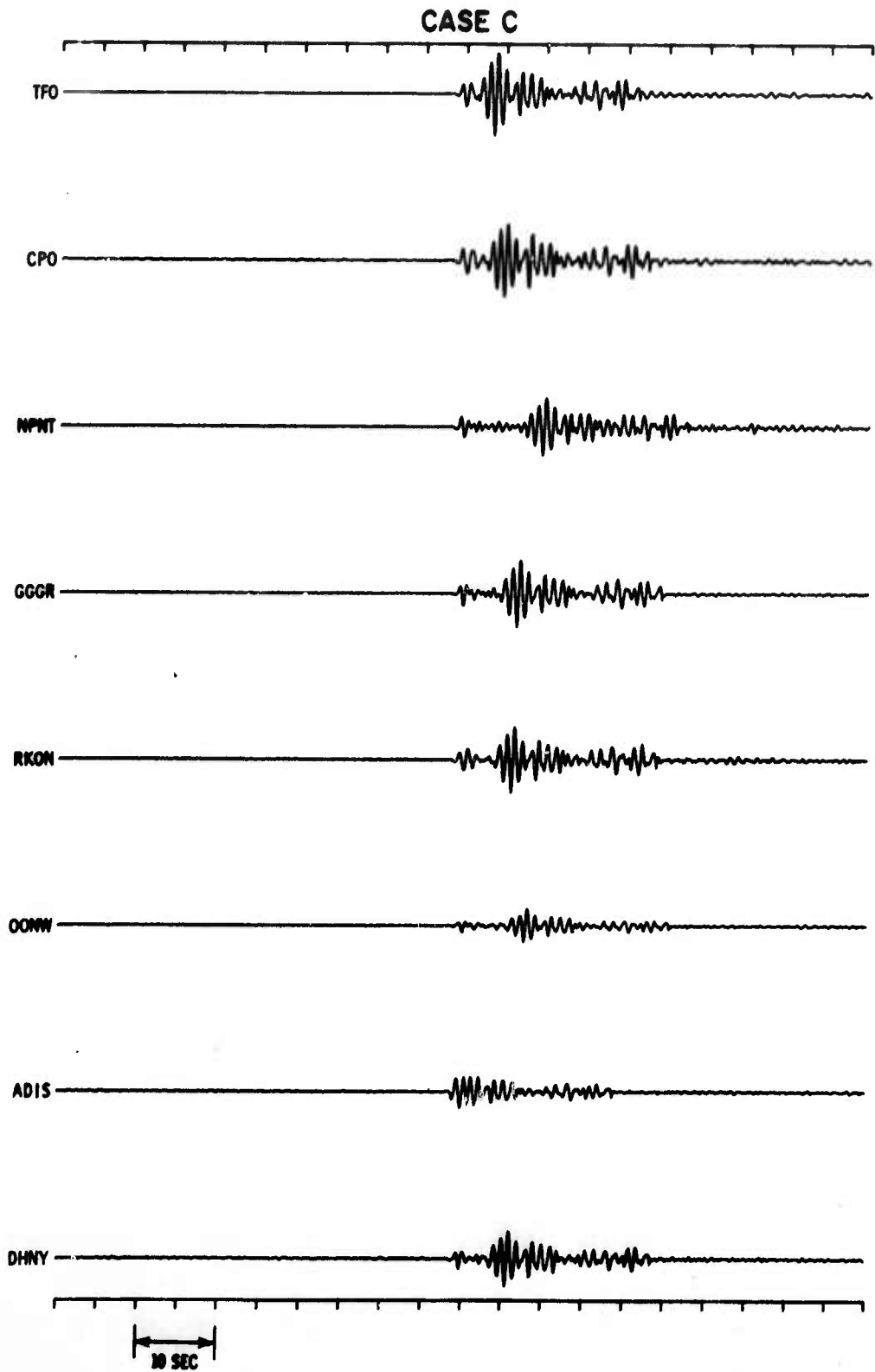


Figure V-3. Case C — Simulated 8-Station Recording of 5.8- and 5.3-Magnitude Earthquakes Occurring Simultaneously and 1° Apart

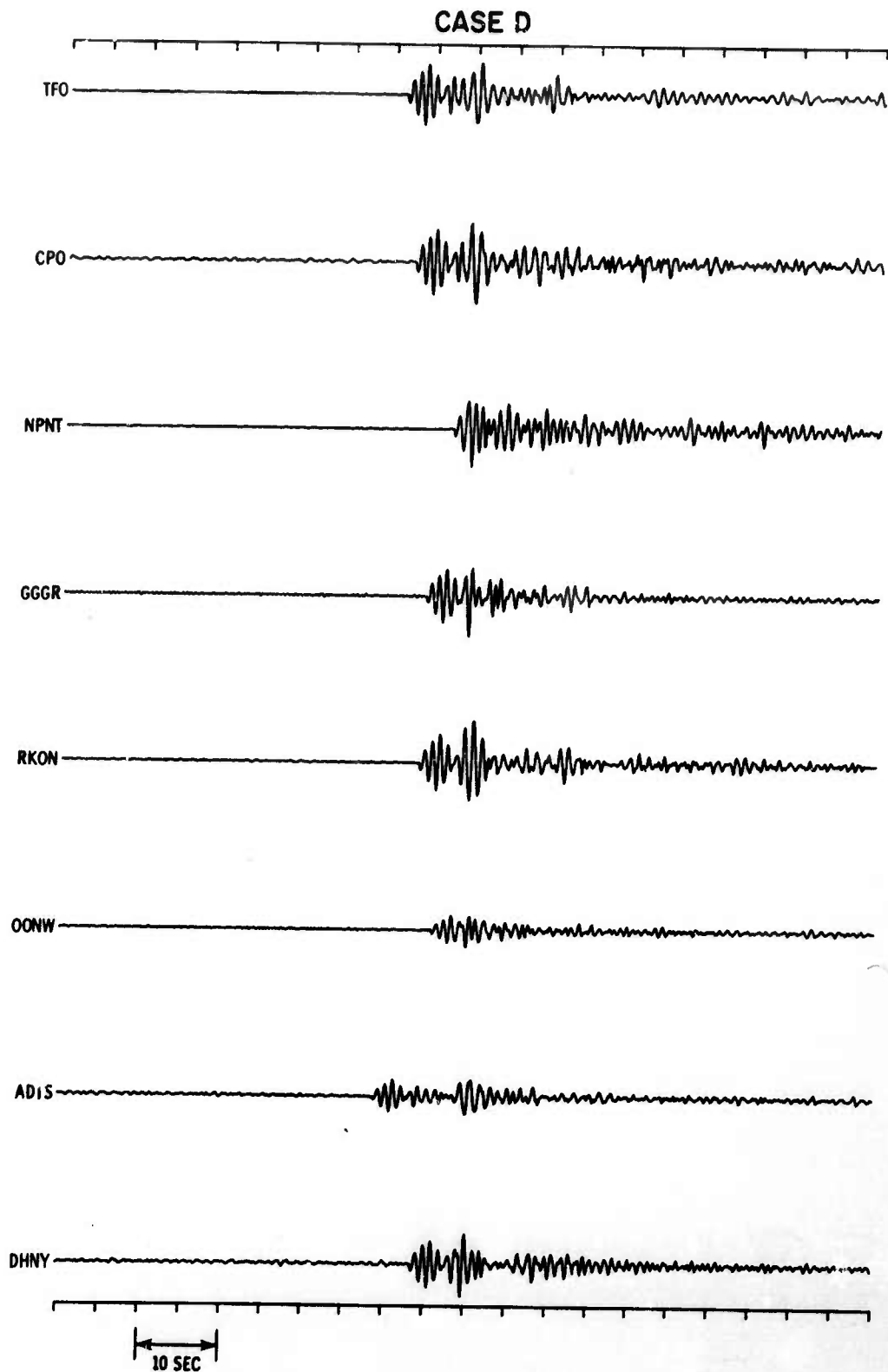


Figure V-4. Case D — Simulated 8-Station Recording of Two 5.8-Magnitude Earthquakes Occurring 10-sec Apart and 1° Apart

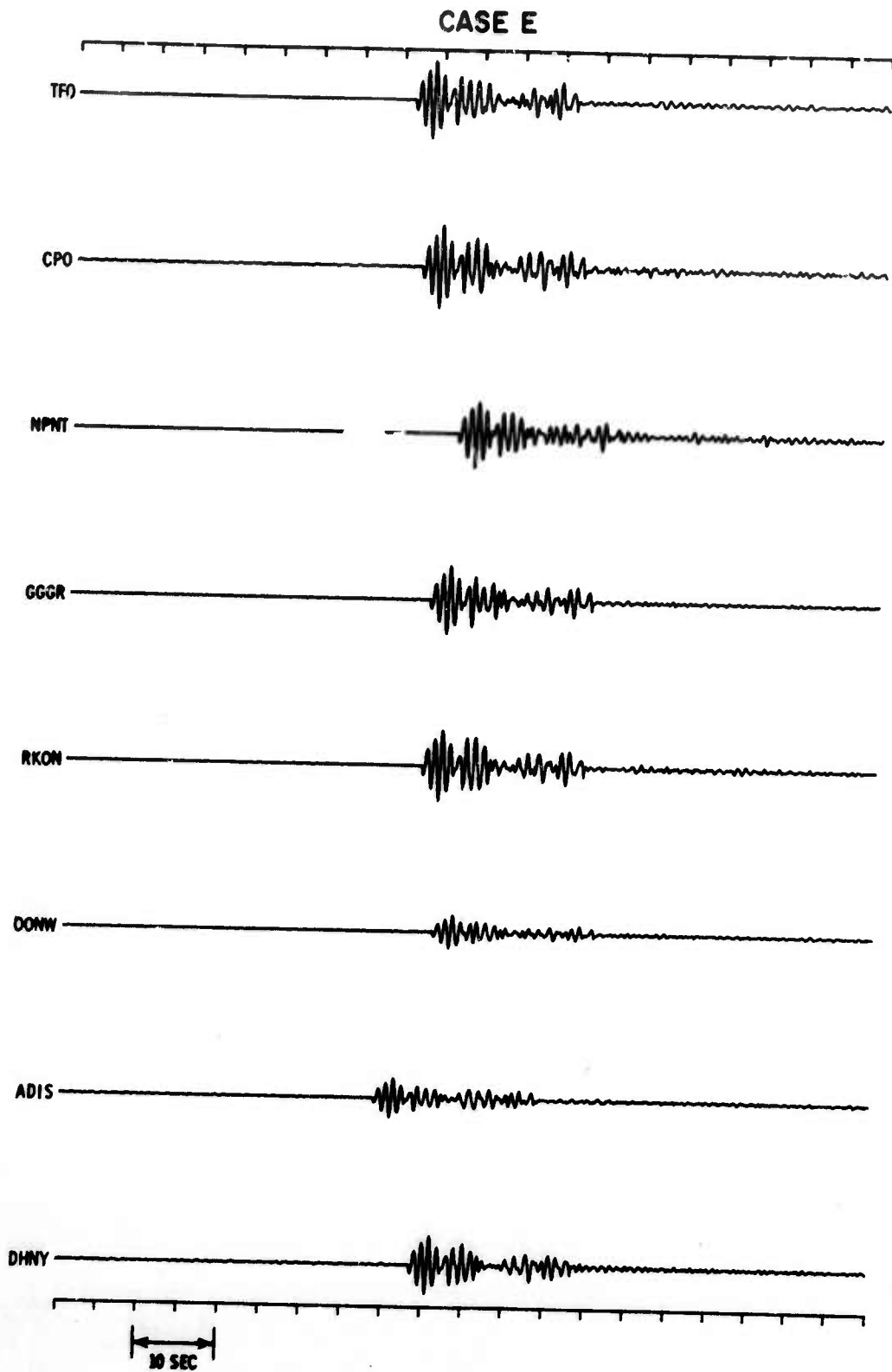


Figure V-5. Case E — Simulated 8-Station Recording of 5.8- and 5.3-Magnitude Earthquakes Occurring 10-sec Apart and 1° Apart

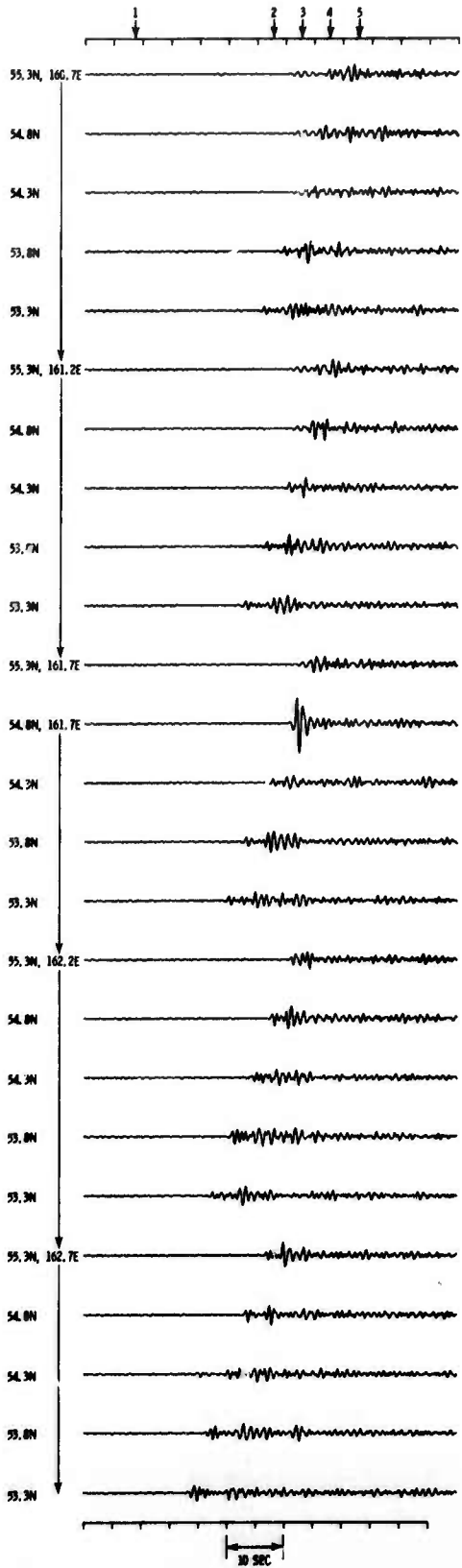


Figure V-6. 8-Station Smoothed Beamsteer Network Outputs for Case A

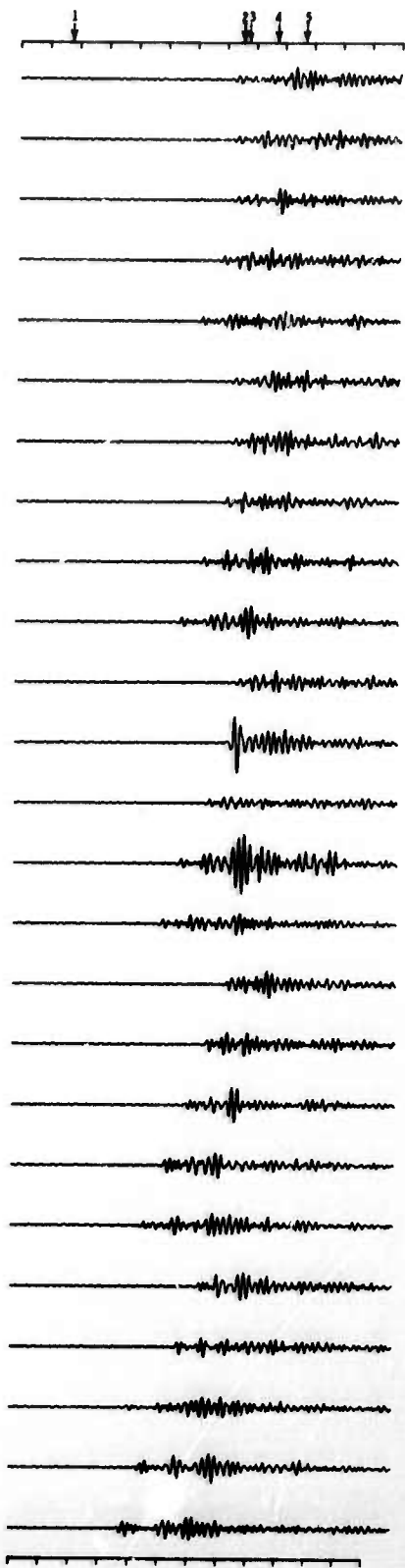


Figure V-7. 8-Station Smoothed Beamsteer Network Outputs for Case B

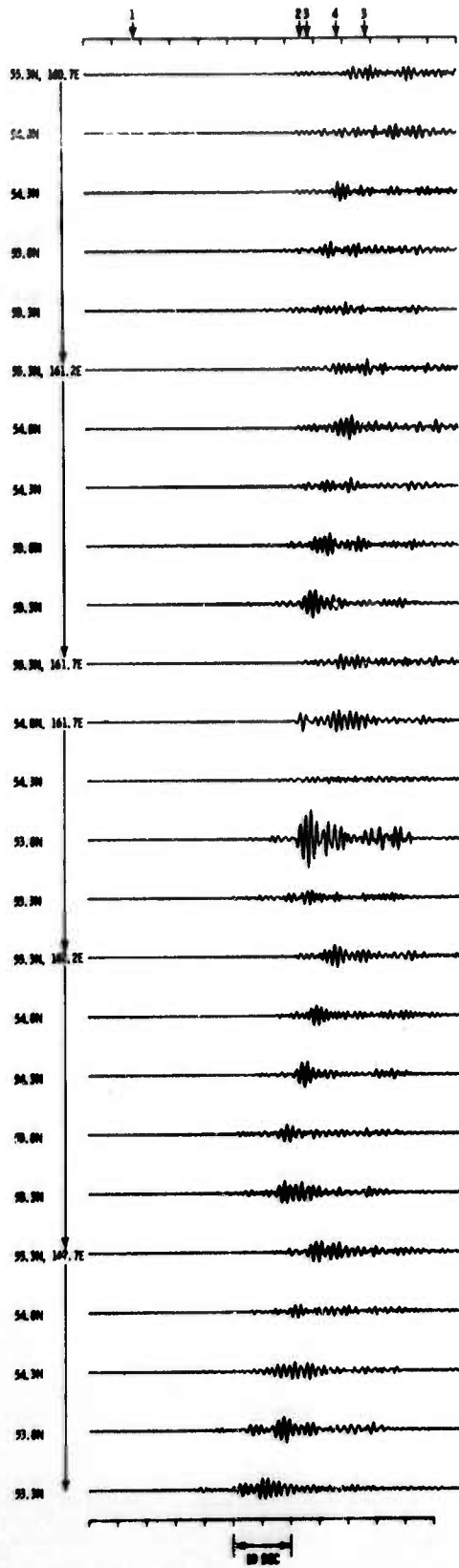


Figure V-8. 8-Station Smoothed Beamsteer Network Outputs for Case C

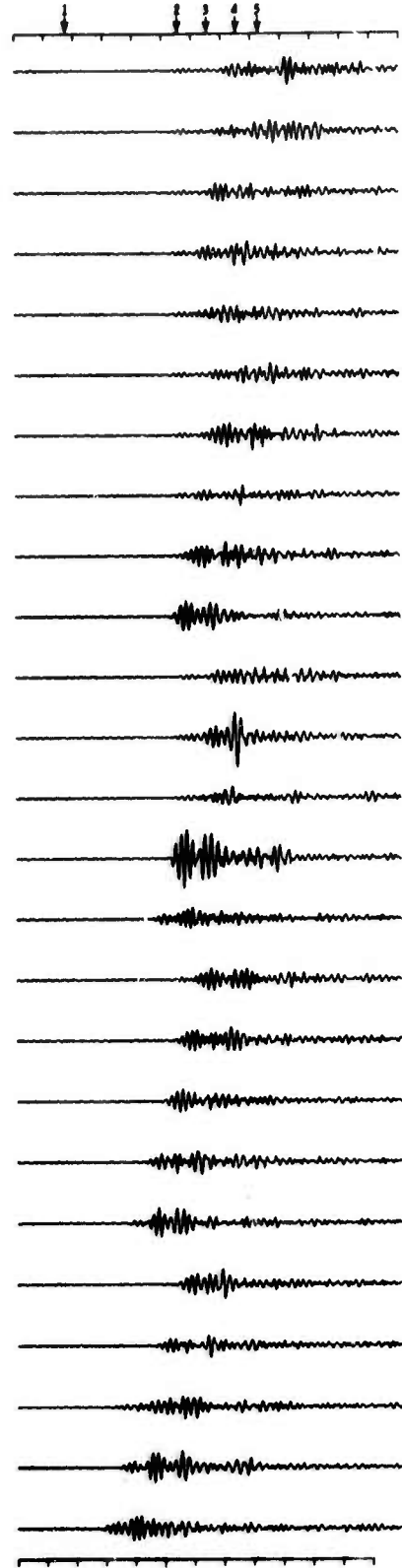


Figure V-9. 8-Station Smoothed Beamsteer Network Outputs for Case D

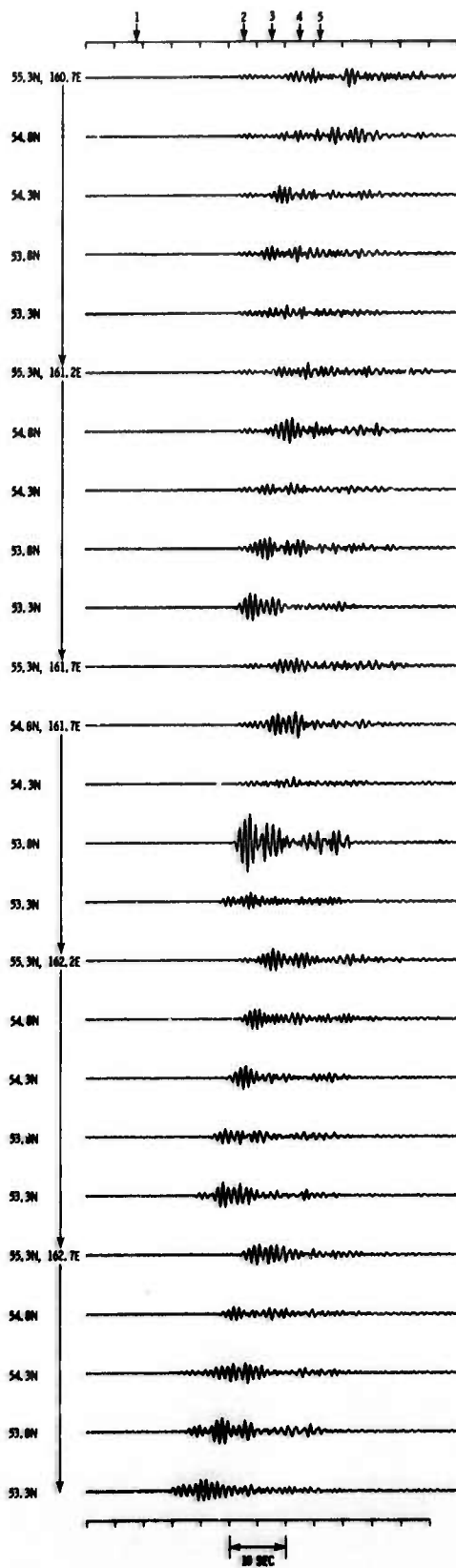


Figure V-10. 8-Station Smoother Beamsteer Network Outputs for Case E



Figure V-11 shows the five beamsteer plots for Case A. This series of plots of total energy in the 2.5-sec gates centered at the times indicated by the numbered arrows on Figure V-6 show the result of a single-event P-wave arrival. Number 1 indicates the ambient noise level preceding the event. Number 2 is taken just prior to the event and illustrates the effect of including a portion of the event in some of the beamsteered outputs. The upper left portion of the plot shows ambient noise levels, while time-shifts for the lower right portion begin to include event energy. The five gates are not equally spaced in time and tend to emphasize this effect, which would be generally characteristic of on-line operation as an event moves in and out of the time gate being examined. Power reaches a relative maximum at the expected arrival time in Number 3. This plot correctly locates the event at 54.8°N , 161.7°E . Numbers 4 and 5 indicate that the P-wave energy from this simple event has already dissipated and the power is returning to the ambient noise level (Number 1).

All plots in Figures V-11 through V-15 are referenced to the maximum power level, which occurs in Number 3, Case C.



CASE A

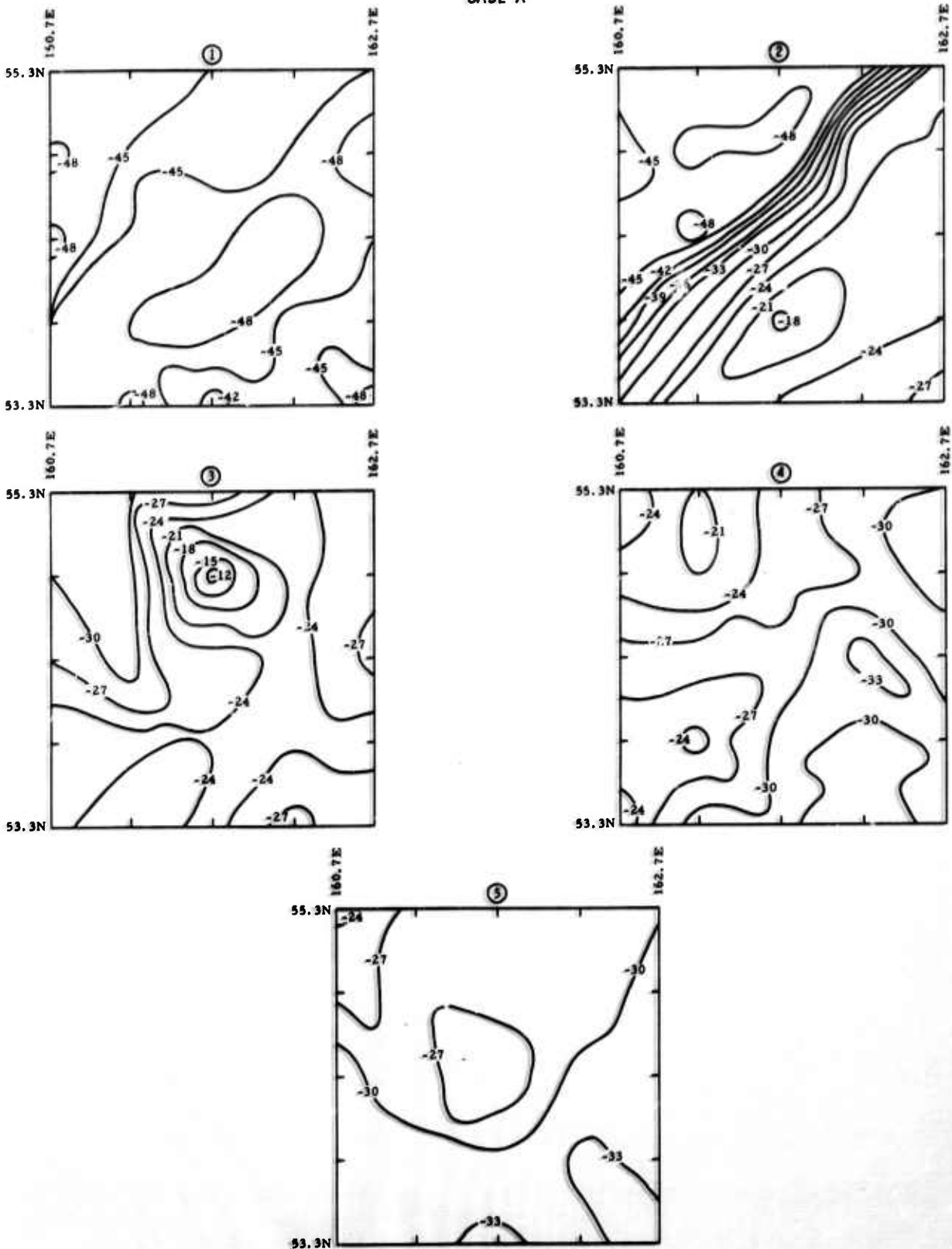


Figure V-11. Beamsteered Plots for Five Time Traces for Case A



Figure V-12 presents the five beamsteer plots for Case B, corresponding to the times indicated by the numbered arrows in Figure V-7. The plots show how well two events of equal magnitude, occurring at the same time, 1° apart, can be resolved. The two epicenters are 54.8°N , 161.7°E and 53.8°N , 161.7°E . Numbers 2 and 3 show energy at these two locations plus slight indication of sidelobe energy at 54.3°N , 162.2°E . Numbers 4 and 5 continue to show energy from the complex event, while no indication of energy from the simple event is evident.



CASE B

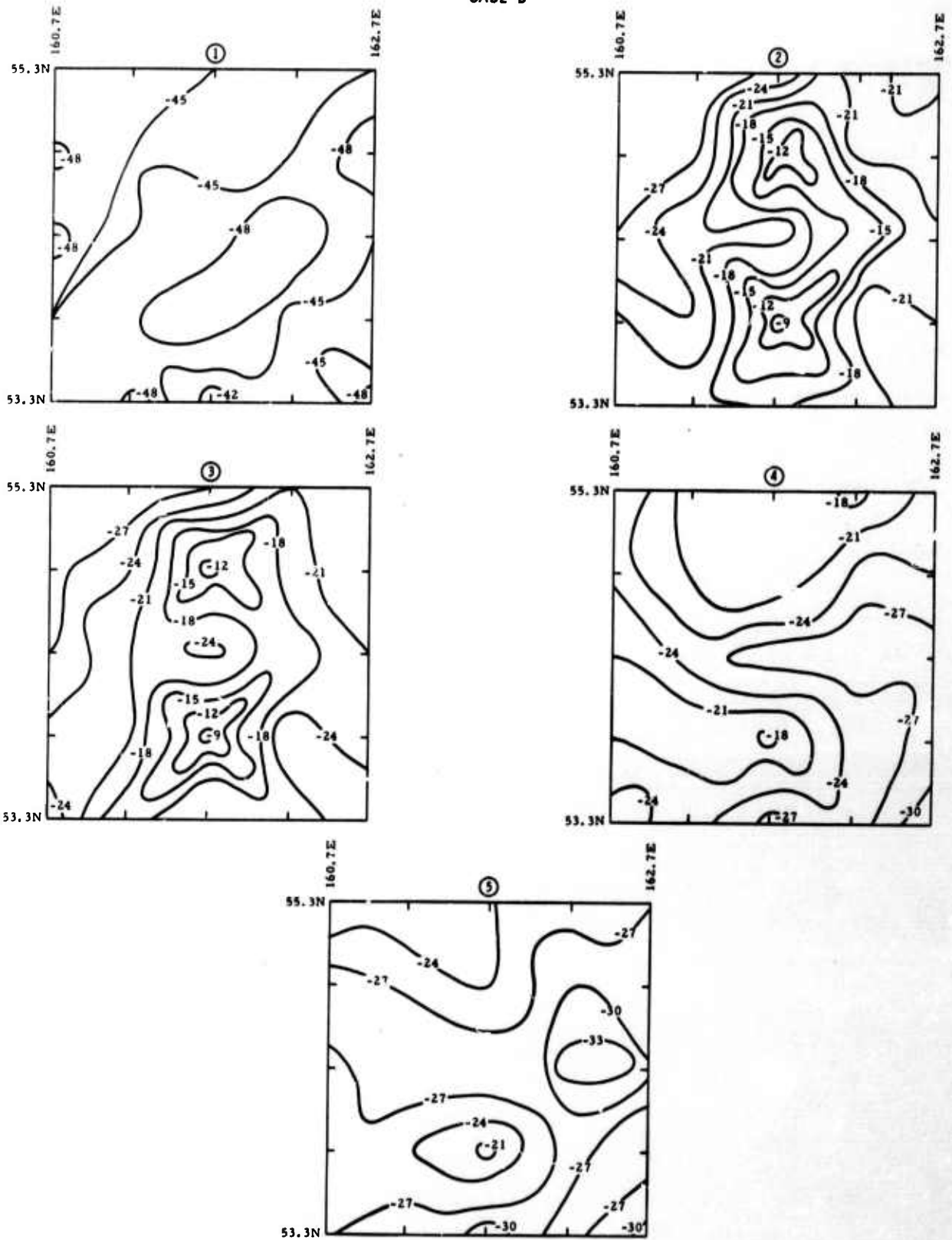


Figure V-12. Beamsteered Plots for Five Time Traces for Case B



The beamsteer plots for Case C are presented in Figure V-13. This multiple-event case is the same as Case B except that the events are not of equal magnitude. The simple event originating at 54.8°N , 161.7°E is one-half magnitude unit lower than the complex event originating at 53.8°N , 161.7°E . Number 2 shows that the weaker event was detected at the correct location about 12 db down from the maximum on the plot corresponding to the stronger event. This plot can be compared to the Case-B plot 2 in Figure V-12. The sidelobe energy, about 6 db down from the maximum, is still present at 54.3°N , 162.2°E and, therefore, must be due to effects from the more complex event. Plot 3 was formed 1.2 sec after plot 2. The larger event has reached its maximum power, and the weak event has completely dissipated. Numbers 4 and 5 show the continued decline of energy from the larger complex event.



CASE C

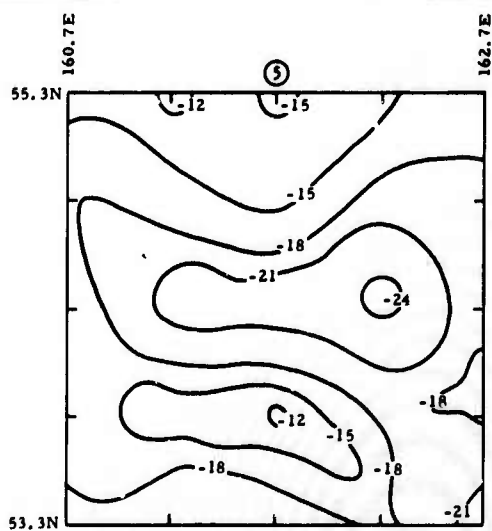
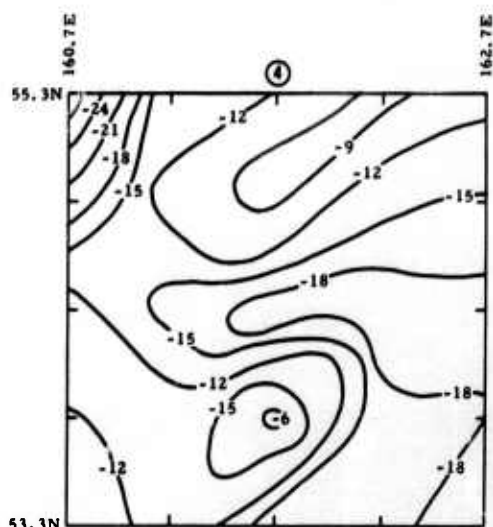
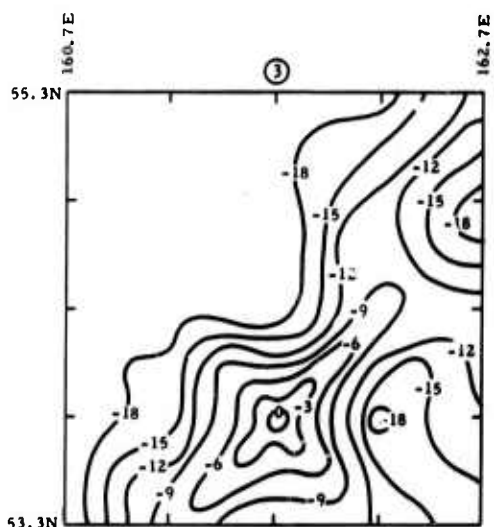
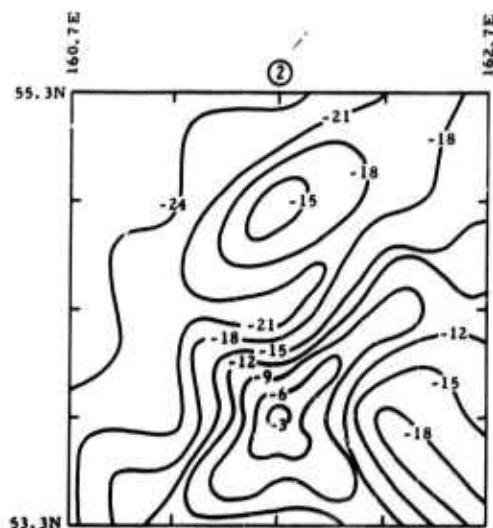
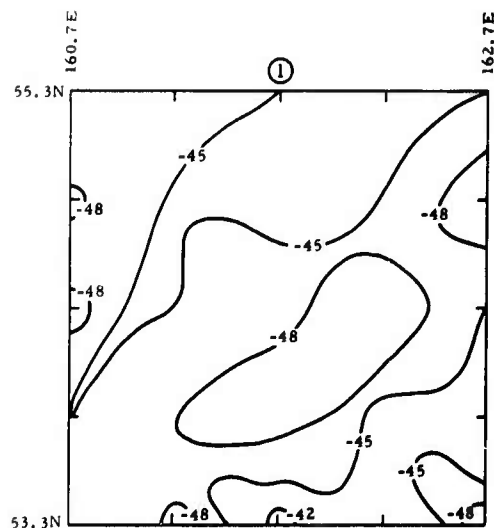


Figure V-13. Beamsteered Plots for Five Time Traces for Case C



Figure V-14 presents the five beamsteer plots for Case D corresponding to the times shown by the numbered arrows in Figure V-9. These plots show resolution of two equal-magnitude events occurring 1° apart, separated in time by 10 sec. The noise plot, Number 1, is nearly identical to the noise plots presented in the preceding cases. Number 2 shows the first event has been detected and correctly located at 53.8°N , 161.7°E . Number 3 shows that the power from this event is dropping off; Number 4, taken 10 sec after Number 2, shows the second event has been detected and correctly located at 54.8°N , 161.7°E . Number 5 indicates that evidence of the second event has disappeared almost completely, while energy from the first, more complex, event is still slightly visible.



CASE D

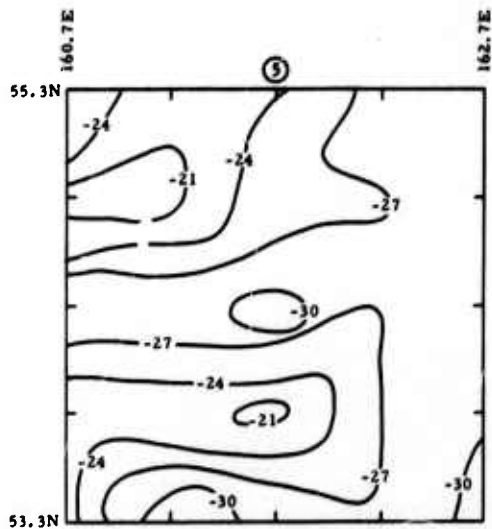
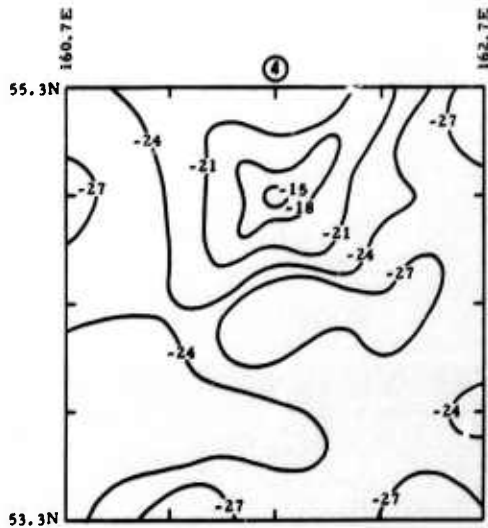
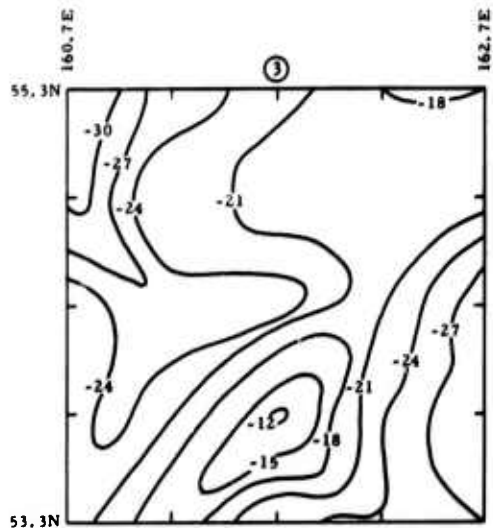
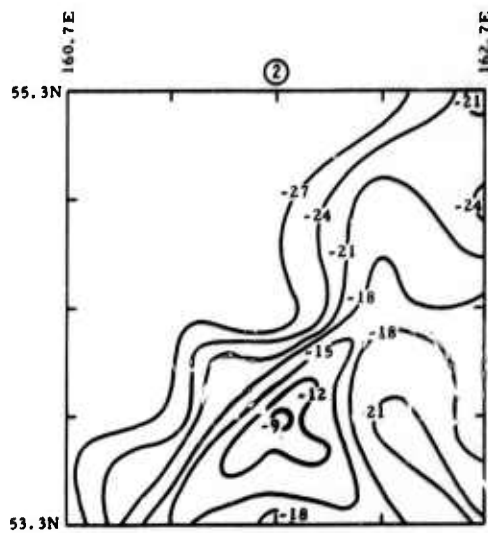
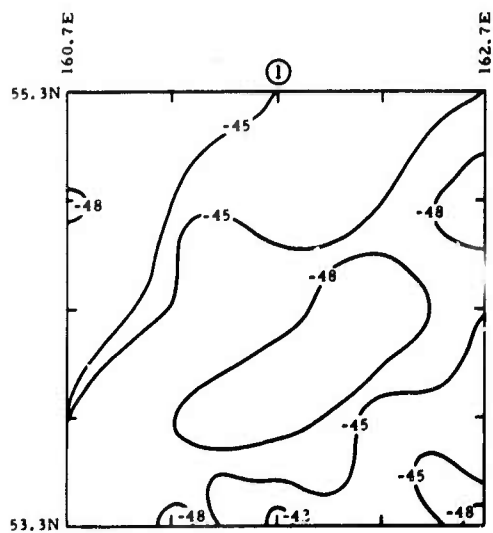


Figure V-14. Beamsteered Plots for Five Time Traces for Case D



The five beamsteer plots for Case E, formed at the times indicated by the numbered arrows in Figure V-10, are presented in Figure V-15. Case E differs from Case D in that the simple event originating at 54.8°N , 161.7°E is one-half magnitude unit lower than the complex event originating 10 sec earlier at 53.8°N , 161.7°E . Numbers 2 and 3 indicate that the larger event has been detected and correctly located. Number 4 formed 10 sec after Number 2, is at the time of the weaker event arrival and shows a slight indication of the event at the correct location. Number 5, taken 5 sec later, shows some energy still present from the stronger event but, as expected, no energy from the simpler event.



CASE E

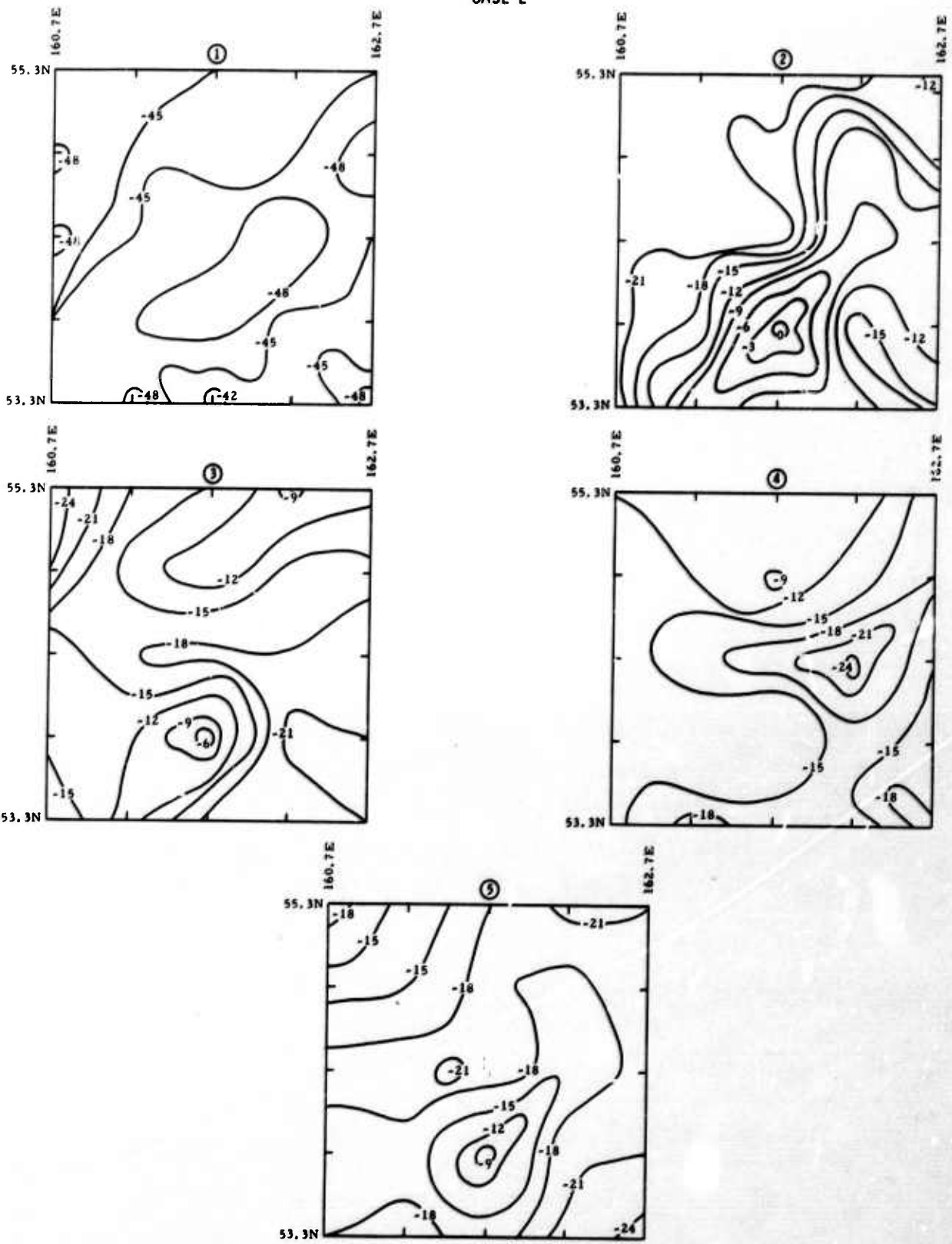


Figure V-15. Beamsteered Plots for Five Time Traces for Case E



Multiple beamsteering of a limited network followed by square-law detection appears to be an effective technique for detecting and resolving time-overlapping events when the two events do not differ in magnitude by more than one-half magnitude units. The lower-magnitude event was always the simple event. Events with larger variations in magnitude undoubtedly could be separated if they occurred farther apart or were more nearly of the same degree of complexity. A more extensive network could be used to detect simple explosions buried in complex larger-magnitude earthquakes and to detect and locate small aftershocks from the earthquake.

Future experiments of this type should determine the maximum magnitude difference as a function of epicenter separation for which effective event resolution can be achieved. The effects of traveltime anomalies and variation in signal-to-noise ratios among stations also should be investigated.



SECTION VI
EVALUATION OF A TECHNIQUE FOR
WORLDWIDE COHERENT ENERGY ANALYSIS

A technique which could be used in a real-time processing system for locating coherent seismic energy sources on a worldwide basis was evaluated. This technique was chosen for processing because of its simplicity and, thus, minimum processing cost. It is basically a time-shift-and-sum (beamsteer) technique performed in the frequency domain. Such a technique would be valuable because of the substantial data reduction and ease of interpretation achieved. The technique probably would have limited use with short-period data because of the time-anomaly problem; however, it would be useful for long-period data which are relatively insensitive to time anomalies.

The time-shift-and-sum output $g(t)$ of N time functions $g_i(t)$ is defined as

$$g(t) = \sum_{i=1}^N g_i(t - \tau_i)$$

where the τ_i 's are the time shifts necessary to align the P-waves for the hypothesized epicenter.

The time-domain function $g(t)$ may be expressed in the frequency domain by computing its Fourier transform; i. e.,

$$G(f) = F [g(t)]$$



Since a Fourier transform is a linear operation, the transform of $g(t)$ may be expressed as

$$G(f) = F \left[\sum_{i=1}^N g_i(t - \tau_i) \right] = \sum_{i=1}^N F \left[g_i(t - \tau_i) \right]$$

Writing the transform of $g(t)$ as an integral and defining the transform of $g_i(t)$ to be $G_i(f)$ yields

$$\begin{aligned} G(f) &= \sum_{i=1}^N \int_{-\infty}^{\infty} g_i(t - \tau_i) e^{-j2\pi ft} dt \\ &= \sum_{i=1}^N e^{-j2\pi f\tau_i} \int_{-\infty}^{\infty} g_i(t - \tau_i) e^{-2\pi f(t - \tau_i)} d(t - \tau_i) \\ &= \sum_{i=1}^N e^{-j2\pi f\tau_i} G_i(f) \end{aligned}$$

The technique was evaluated with synthesized frequency-domain data representing a simulated 20-station worldwide network. The data consisted of complex representations of power at a given frequency, each rotated through a certain phase angle determined by the epicentral distance between the simulated source and a particular network station. Each station of the simulated network was considered to be located at one of the vertices of a dodecahedron inscribed in a spherical model of the earth, with one of the vertices located at the North Pole. All arrival times used to compute time shifts were based on the Jeffreys-Bullen traveltime tables. The synthetic Fourier transforms constructed for each station simulated a P-wave source located at the North Pole. The transforms were designed to simulate both short and long-period signals with frequencies of 1.0 Hz and 0.05 Hz, respectively, and to have unity power at each station.



The worldwide display of beamsteers formed using this network consisted of two parts. Each was a circular grid of points representing the projection of a hemisphere onto a plane, with the North (or South) pole at the center. Longitude appeared as straight lines radiating from the center, while latitude appeared as concentric circles. For each point in the grid, epicentral distances to each station and the corresponding Jeffreys-Bullen traveltimes were computed, excluding those stations at epicentral distances greater than 104° from the point. The traveltimes were used to determine relative time shifts which then were applied to the simulated station data (as described earlier), aligned, and summed.

In general, the display may be centered at any point on the earth's surface and may extend to any radius up to 90° . Only when the display center is located at one of the poles do the latitude and longitude lines behave as described earlier. The projection generally may be considered as that of a spherical surface onto one end of a right cylinder (of radius R , when $R \leq 90^\circ$), with the long axis passing through the center of the earth.

Contour plots were formed using the measured power obtained by beamsteering at each point in the grid. All displayed contour plots are referenced to their maximum power and have an asterisk at the 0-db point. Shaded areas represent power levels less than 0 db and greater than or equal to -3 db. Areas enclosed by contour lines are less than -3 db and greater than or equal to -6 db. Contouring was performed only down to -6 db to simplify the display. In general, power levels outside the contoured areas are -12 db or lower. Only northern-hemisphere plots are shown because the simulated source is located at the North Pole, thus the southern-hemisphere plots showed no peaks and a generally low power level.



Contour plots for the 20-station simulated network using short-period and long-period signals are shown in Figures VI-1 and VI-2, respectively. Also for the simulated network, a contour plot of a long-period signal with synthetic time residuals is shown in Figure VI-3. Standard deviation of the random, normally distributed time residuals was 0.5 sec. The contour plot for a simulated long-period signal obtained using the existing 10-station worldwide array is shown in Figure VI-4.

All of the short-period and long-period contour plots indicate maximum power at the North Pole, thus locating the simulated signal properly. Relatively small, station time residuals introduced for one long-period plot do not cause the source to be mislocated. The one outstanding feature observed for all plots is the presence of numerous sidelobe peaks which are only 0 to 6 db down from the main lobe. Such sidelobe patterns would make it difficult to distinguish overlapping signals from different sources.

Figure VI-5 displays the spectrum of two overlapping events as would be obtained from short-period data recorded with the 8-station network discussed in Section V. Transforms were generated to simulate two sources 1° apart with geographic locations of 53.8°N , 161.7°E and 54.8°N , 161.7°E . Contour plots are shown for events from the individual sources and for simultaneous occurrence of the two events. These contour plots are for a small area of the earth's surface, 1° in radius, centered about a point equidistant from the two events.

The single-event spectra locate the events properly but exhibit severe sidelobes. When the two sources are combined, maximum power is not found at either source location; sidelobes from each source reinforce each other, making it impossible to locate either source properly. The origin of the severe sidelobe problem with the technique currently used is believed to be caused by the ambiguity in relative phase between two stations. The relative phase is $\theta + n2\pi$ radians, where n is unknown and has no effect on the frequency-domain beamsteer. This loss of information which would not occur in time-domain beamsteering leads to higher sidelobes.



This technique is able to locate events isolated in time for perfectly equalized signals. However, if the event is not well-equalized, it would probably be difficult to distinguish between the actual source location and the sidelobes. For the time-overlapping event case, sidelobe patterns for each of the events reinforce each other and make separating the events impossible. However, based on the technique's ability to locate equalized signals correctly and to be unaffected by time anomalies for the long-period case, variations of such techniques — all leading to the same type of power-density vs geographical-position display — should be investigated.

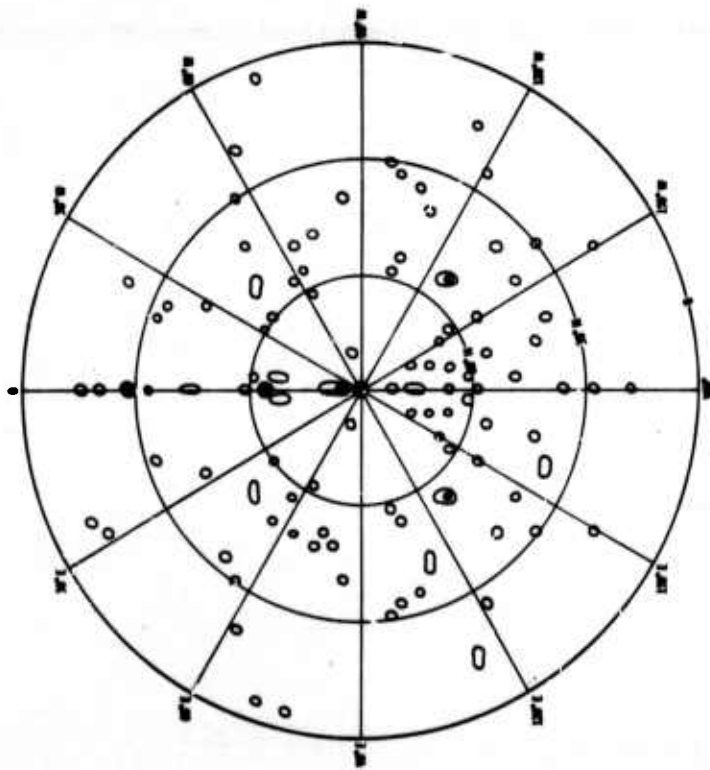
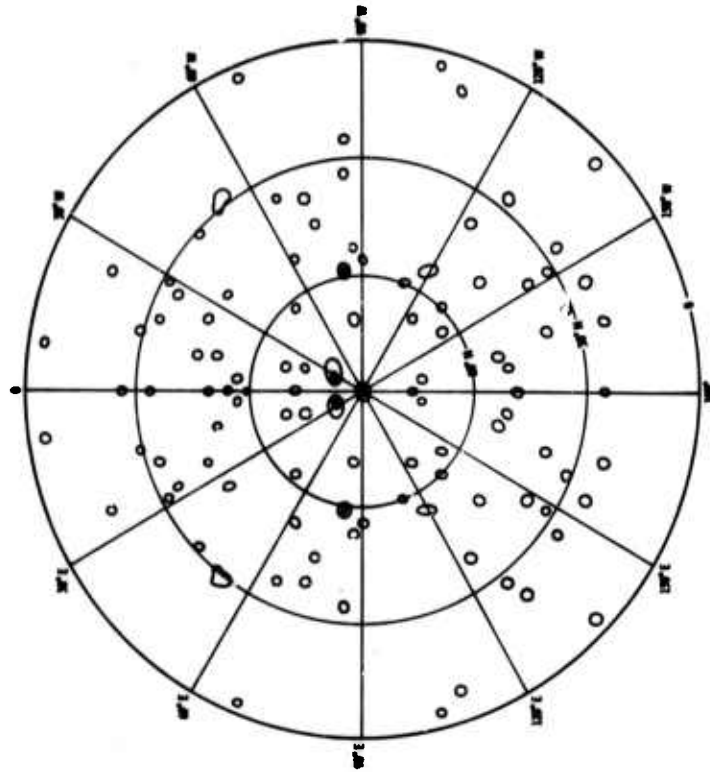


Figure VI-1. Worldwide Spectrum, Short-Period Equalized Signal ($f = 1.0$ Hz, maximum power at center)

Figure VI-2. Worldwide Spectrum, Long-Period Equalized Signal ($f = 0.05$ Hz, maximum power at center)

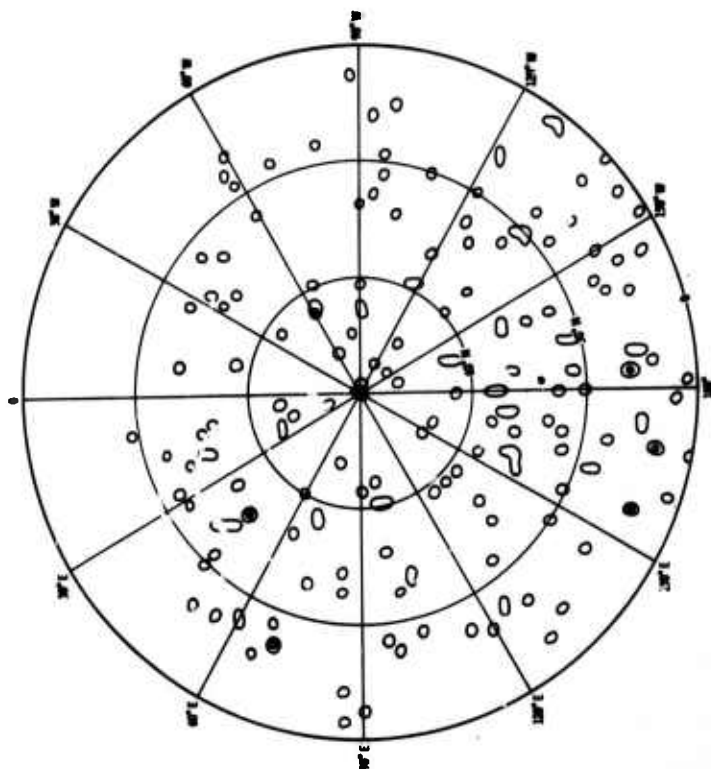


Figure VI-4. Worldwide Spectrum, Long-Period Equalized Signal with Existing 10-Station Network ($f = 0.05$ Hz, maximum power at center)

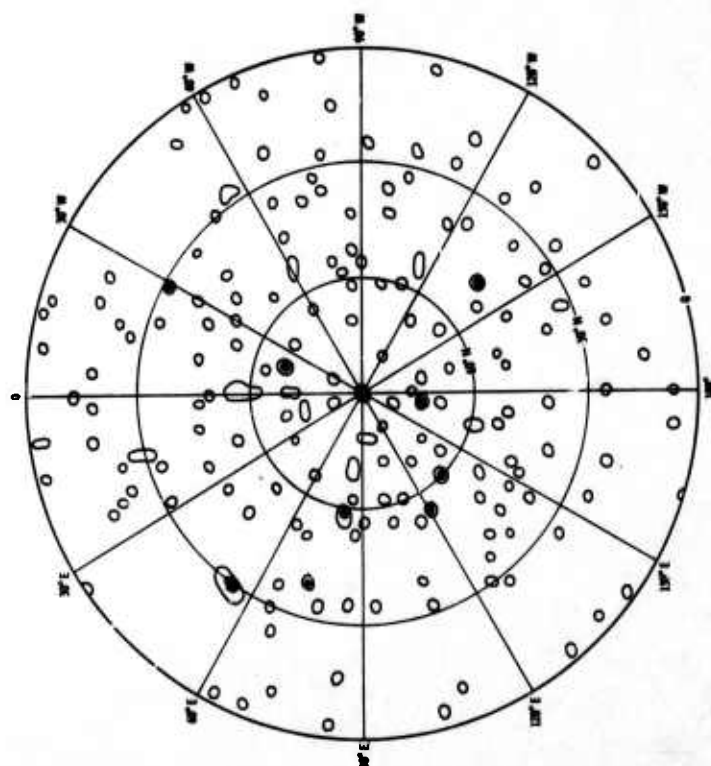


Figure VI-3. Worldwide Spectrum, Long-Period Equalized Signal with Time Residuals ($f = 0.05$ Hz, maximum power at center)

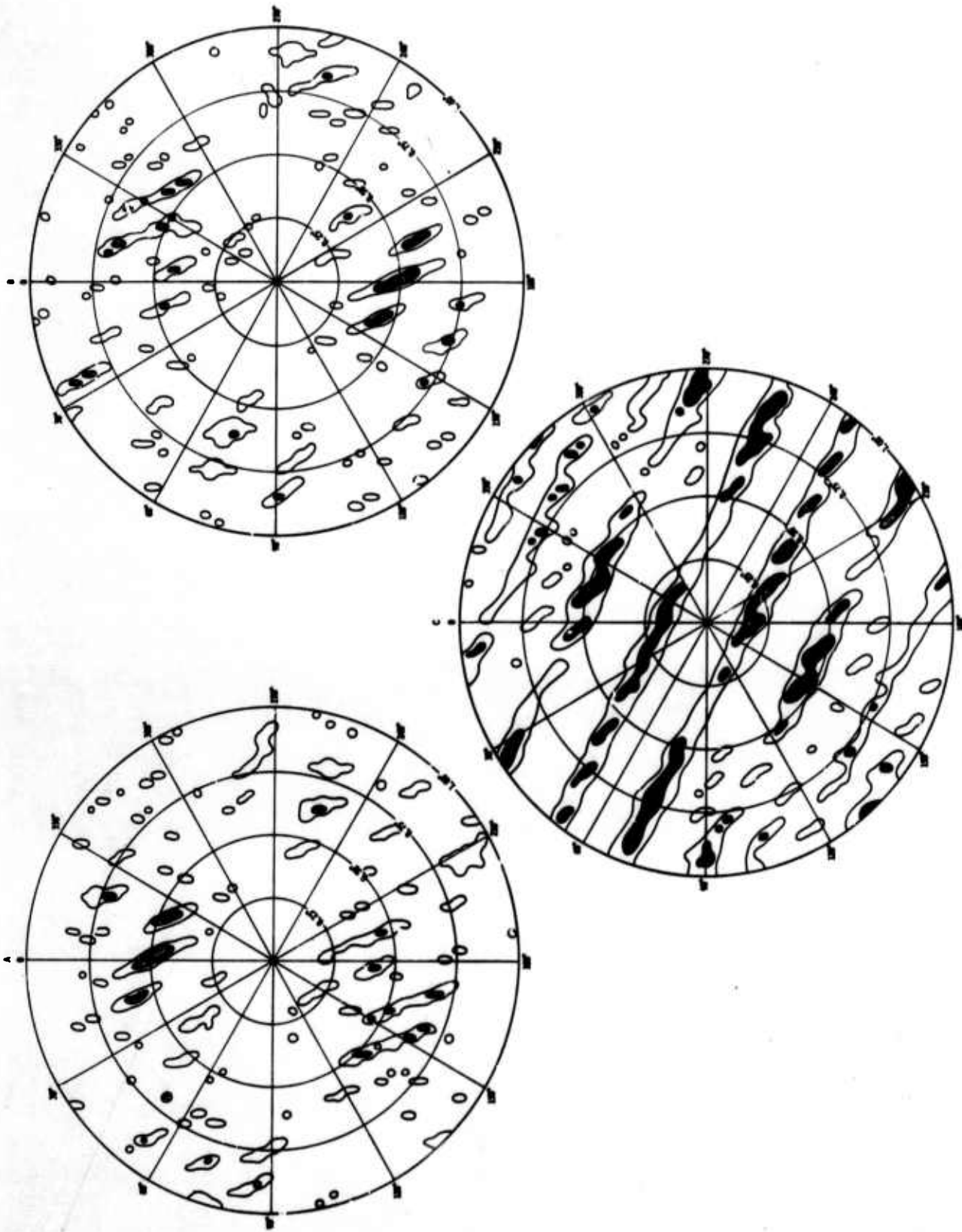


Figure VI-5. Worldwide Spectrum, Two Time-Overlapping Short-Period Equalized Signals ($f = 1.0$ Hz)

UNCLASSIFIED

Security Classification

DOCUMENT CONTROL DATA - R & D

(Security classification of title, body of abstract and indexing annotation must be entered when the overall report is classified)

1. ORIGINATING ACTIVITY (Corporate author) Texas Instruments Incorporated Science Services Division P. O. Box 5621 Dallas, Texas 75222	2a. REPORT SECURITY CLASSIFICATION Unclassified
	2b. GROUP -

3. REPORT TITLE
NETWORK STUDIES — SIGNAL CHARACTERISTICS
ADVANCED ARRAY RESEARCH — SPECIAL REPORT NO. 7

4. DESCRIPTIVE NOTES (Type of report and inclusive dates)
Special

5. AUTHOR(S) (First name, middle initial, last name)
Johnson, William A. Bonner, James A.
Strange, Peter L. Benno, Stephen A.

6. REPORT DATE 15 February 1968	7a. TOTAL NO. OF PAGES 81	7b. NO. OF REFS 2
------------------------------------	------------------------------	----------------------

8a. CONTRACT OR GRANT NO. F33657-67-C-0708-P001 b. PROJECT NO. VELA T/7701 c. d.	9a. ORIGINATOR'S REPORT NUMBER(S) —
	9b. OTHER REPORT NO(S) (Any other numbers that may be assigned this report) —

10. DISTRIBUTION STATEMENT
This document is subject to special export controls, and each transmittal to foreign governments or foreign nationals may be made only with prior approval of Chief, AFTAC.

11. SUPPLEMENTARY NOTES ARPA Order No. 624	12. SPONSORING MILITARY ACTIVITY Advanced Research Projects Agency Department of Defense The Pentagon, Washington, D. C. 20301
---	---

13. ABSTRACT
This report presents an initial study of signal characteristics and coherent signal processing at the network level. Topics investigated include signal similarity, depth-phase detection and recognition, separation and location of events overlapping in time and space, and methods for real-time network processing and data presentation. Large variations in signal waveform and signal-to-noise ratio (SNR) are observed across the network. Interstation coefficients of correlation for a relatively simple Kamchatka event vary from 0.54 to 0.96, with the higher correlation found for stations on the eastern North American continent. Levinson equalization filtering does not appear particularly effective at the network level in terms of improved correlation coefficients or SNR. Depth-phase detection at the network level is not materially better than for selected stations, but recognition appears more reliable than for general station results. Experiments show that overlapping events of differing magnitudes and separated in epicenter by as little as 1° can be resolved by network beamsteer and integrate techniques. Signal-enhancement procedures implemented primarily to determine the extent of signal attenuation caused by signal dissimilarity across the network indicate less than 3-db reduction in signal energy across the signal passband. Ambient noise levels and scattered signal in the P coda are reduced by 7 to 9 db, as expected for uncorrelated energy. A method of weighting stations by their SNR's emphasizes the stations with better signal estimates and yields an additional 4 to 7 db improvement in SNR at the network level.

14.

KEY WORDS

LINK A

LINK B

LINK C

ROLE

WT

ROLE

WT

ROLE

WT

Advanced Array Research

Network Studies

Signal Characteristics

Beamsteer and Integrate Techniques

Signal Similarity

Depth-Phase Detection and Recognition

Separation and Location of Events

Overlapping in Time and Space

Real-Time Network Processing and

Data Presentation